Predicting dominance of sand transport by waves, tides and their interactions on sandy continental shelves

E. V. King[1, 2], D. C. Conley[1], G. Masselink[1], N. Leonardi[3]

[1]Coastal Processes Research Group, School of Biological and Marine Sciences, University of Plymouth, Plymouth, UK.

[2]Scottish Environment Protection Agency, Glasgow, Scotland, UK.

[3]Department of Geography and Planning, School of Environmental Sciences, University of Liverpool, Liverpool, UK.

Corresponding author: Erin King (erin.king@plymouth.ac.uk, erin.king@sepa.org.uk)

Key Points:

- Dominant forcing mode and magnitude of net sand transport is predictable from readily available data using a k-Nearest Neighbour algorithm.
- Sand waves increase in length and asymmetry, and decrease in height, for increasing wave-dominance under extreme conditions.
- Over an average year, meso-macrotidal areas are tide-dominated, while shallow, finer grained, microtidal regions are wave-dominated.

Key Words:

Sand Transport, Sediment Transport, Wave-Current Interaction, Continental Shelf, k-Nearest Neighbour, Sand Waves, Classification Scheme

Abstract

Waves and tidal currents resuspend and transport shelf sediments, influencing sediment distributions and bedform morphology with implications for various topics including benthic habitats, marine operations, and marine spatial planning. Shelf-scale assessments of wave-tide-dominance of sand transport tend not to fully include wave-tide interactions (WTI), which non-linearly enhance bed shear stress and apparent roughness, change the current profile, modulate wave forcing, and can dominate net sand transport. Assessment of the relative contribution of WTI to net sand transport requires computationally/ labour intensive coupled numerical modelling, making comparison between regions or climate conditions challenging. Using the Northwest European Shelf, we show the dominant forcing mode and potential magnitude of net sand transport is predictable from readily available, uncoupled wave, tide and morphological data in a computationally efficient manner using a k-Nearest Neighbour algorithm. Shelf areas exhibit different dominant forcing modes for similar wave exceedance conditions, relating to differences in depth, grain size, tide range, and wave exposure. WTI dominate across most areas in energetic combined conditions. Over a statistically representative year, meso-macrotidal areas exhibit tide-dominance, while shallow, finer grained, amphidromic regions show wave-dominance, with WTI dominating extensively >30m depth. Seabed morphology is strongly affected by sediment transport mode, and sand wave geometry varies significantly between predicted dominance classes with increased length and asymmetry, and decreased height, for increasing wave-dominance. This approach efficiently indicates where simple non-interactive wave and tide processes may be sufficient for modelling sediment transport, and enables efficient inter-regional comparisons and sensitivity testing to changing climate conditions with applications globally.

Plain Language Summary

The net transport of sand across the continental shelf is important to understand. It influences the transport and fate of sediments, pollutants, and can affect seabed habitats. Net sand transport results from tide and wave action, and these forces interact in a non-linear way in combined wave-tide conditions. Calculating the magnitude and dominant forcing (waves, tides or wave-tide interactions) requires complex modelling which takes time and resources. Here we show we can predict the magnitude and dominant forcing using a k-Nearest-Neighbour algorithm trained with readily available data for the Northwest European Shelf. Different forces drive net sand transport depending on depth, grain size, tide range and wave exposure. Areas with the largest tides show tide-dominance over a year, while shallow areas with finer sand and exposure to energetic waves show wave-dominance. We show that sand wave length and asymmetry increase whilst height decreases for increased wave-dominance during storms.

1. Introduction

Residual (net) sediment transport patterns influence the transport and fate of continental shelf sediments, influencing sediment distributions and morphological evolution (Harris & Collins, 1991; King et al., 2019; Leonardi et al., 2017; Pingree & Griffiths, 1979; Pingree & Le Cann, 1989; Stride, 1963; van der Molen, 2002; Xu et al., 2016; Zhang et al., 2016). Waves and tidal currents result in resuspension and transport of shelf sediments (Carter & Heath, 1975; Pattiaratchi & Collins, 1988; Thompson et al., 2019), influencing sand wave morphology (Damen et al., 2018; Wang et al., 2019) with implications for marine spatial planning of pipelines and cables for windfarms and offshore renewable energy (Cheng et al., 2020; Németh et al., 2003; Roetert et al., 2017), dispersal of contaminants (e.g. dredge disposal; Cieślikiewicz et al., 2018; Uncles et al., 2020), and the fate of shoreface nourishments (Luijendijk et al., 2017). Shear stresses and sand transport driven by tides and waves influence benthic communities through disturbance, whilst also acting as a vector for recolonization (Aldridge et al., 2015; Bricheno et al., 2015; Dernie et al., 2003; Hall, 1994; Harris, 2014; Levin, 1995; Reiss et al., 2010). The relative impact of wave and tidal forcing influences sand wave morphology and migration rates (Campmans et al., 2018a,b; Damen et al., 2018; Van Dijk & Kleinhans, 2005), causing potential disturbance and affecting the distribution of benthic communities (Damveld et al., 2018; 2020; Harris, 2014). Predictive habitat suitability modelling requires an understanding of physical disturbance regimes and knowledge of the dominant drivers of sand transport at the shelf scale is important (Harris, 2014).

Assessments of the relative impact of waves and tidal currents on the bed across sandy continental shelves have been conducted. Bricheno et al. (2015) map the relative impact of tides and storm events at the bed across the NW European Shelf over a 10-year period. South West exposed coasts and shallow water areas were found to be most at risk from large waves and thus are most likely to show wave dominated transport, and modelling suggests the maximum benthic force is wave dominated (Bricheno et al, 2015). The detailed distribution of physical disturbance shows a complex relationship between depth, tidal stress, wave fetch and grain size, with large uncertainty (Aldridge et al., 2015). Porter-Smith et al. (2004) classify the Australian continental shelf based on sediment threshold of motion exceedance from tidal currents and swell waves with classes ranging through waves-only, wave-dominated, mixed, tide-dominated and tide-only. Van der Molen (2002) considers the relative impact of waves, winds and tides on sand transport in the Southern North Sea. However, at present, shelf scale analyses of dominant forcing modes for sand transport do not consider wave-tide interactions. Wave-tide interactions (WTI) non-linearly enhance bed shear stress and apparent roughness due to interaction between wave and tidal bottom boundary layers, influence the vertical current profile and modulate wave forcing through tidal elevation changes (Fredsøe, 1984; Grant &

Madsen, 1979, 1986; Hopkins et al., 2015; Kemp & Simmons, 1982, 1983; Klopman, 1994; Nielsen, 1992; Olabarrieta et al., 2010; Tambroni et al., 2015; Umeyama, 2005).

Boundary layer processes dominated by WTI are fundamentally different from those dominated by either waves or tides, and WTI can dominate net sand transport across large areas of the shelf over a tidal cycle (King et al., 2019). Analyses excluding WTI may underestimate net sand transport under combined wave and tide conditions where WTI can dominate. A classification scheme was proposed by King et al. (2019) for net sand transport per tidal cycle to account for contributions of waves, tides and WTI (accounting for radiation stresses, Stoke's drift, enhanced bottom-friction and bed shear stress, refraction, current-induced Doppler shift, tidal modulation of wave heights and wave blocking); however, this currently requires computationally expensive coupled numerical modelling to assess. A computationally efficient method to assess the dominant sand transport mode and magnitude will enable efficient inter-regional comparison of the role of waves, tides and WTI on sand transport at scale and under varied or changing climate forcing. This enables efficient assessment of where simple non-interactive wave and tide processes may be sufficient to model sediment transport, particularly relevant where application of a model or parameterisation is predicated on dominance of waves (e.g., parameterisations of headland bypassing; King et al., Under Review; McCarroll et al., Under Review), or tides (e.g., models of sand wave morphological evolution in tide-dominated environments; Besio et al., 2007). It also enables efficient assessment of the role of combined wave and tidal processes on seafloor morphology, such as by comparing dominant processes with observed sand wave geometries (e.g., Damen et al., 2017, 2018). It is therefore beneficial to develop a means to quickly assess the dominant sand transport mode on sandy continental shelves without the need for computationally expensive numerical modelling.

This study aims to apply a data driven method to predict the dominant sand transport drivers and sand transport magnitude on sandy continental shelves using the classification scheme of King et al., (2019). This will allow assessment of the importance of WTI to sand transport on sandy continental shelves with a computationally efficient method versus fully coupled hydrodynamic modelling. To achieve this aim we will pursue the following objectives: (i) determine a list of readily available environmental and morphological variables with predictive capacity for the dominant sand transport mode and order of magnitude; (ii) use results of sand transport rates obtained through a validated numerical model to train a k-Nearest Neighbour classifier for dominant sand transport class and order of magnitude; (iii) collate environmental and morphological predictors across a sandy continental shelf with highly varied environmental conditions; and (iv) use the trained kNN classifier to assess the dominant transport mode and sand transport magnitude across the shelf.

2. Methods

2.1. Study region

The Northwest European continental shelf (Figure 1) was selected for this study due to a combination of ready availability of environmental and morphological variables at the shelf scale (Graham et al., 2018; O'Dea et al., 2012; Tonani et al., 2019; Tonani & Saulter, 2020; Wilson et al., 2018), a highly varied tidal regime ranging from macrotidal to microtidal (Pingree & Griffiths, 1979), a varied wave climate ranging from regions exposed to a potential 7000km fetch dominated by long-period swell waves (e.g., Celtic Shelf; Collins, 1987; Draper, 1967; Scott et al., 2016) to regions sheltered from the Atlantic swell and dominated by wind-waves (e.g., Netherlands Shelf; van der Molen, 2002). This continental shelf has a predominantly sand bed with median sand fraction grain size ranging from fine to coarse sand (Figure 1b, c; Wilson et al., 2018). The shelf area has a wealth of literature examining environmental drivers of benthic disturbance (Aldridge et al., 2015; Bricheno et al., 2015; Thompson et al., 2019), sand transport (Harris & Coleman, 1998; King et al., 2019; Leonardi et al., 2017; Pingree & Griffiths, 1979; Uncles, 2010; van der Molen, 2002) and bedform morphodynamics (Cheng et al., 2020; Damen et al., 2018; Ward et al., 2015). These factors make this an ideal region to examine the performance of a method for predicting the dominant driver of sand transport at the shelf scale.

Previous modelling work by King et al. (2019) simulated net sand transport per tidal cycle across a macro-mesotidal section of the Celtic Shelf (Figure 1a) using Delft3D (Booij et al., 1999; Lesser et al., 2004) in a depth-averaged mode using the sand transport formulation of Van Rijn (2007a, b). Delft3D in a depth-averaged mode has previously been used successfully to simulate sand transport processes including WTI on the inner shelf (Hansen et al., 2013; Hopkins et al., 2015; King et al., 2019; Luijendijk et al., 2017; McCarroll et al., 2018; Ridderinkhof et al., 2016). Simulations were performed for spring and neap tides and median and extreme (1% exceedance) waves from two modal directions with all possible combinations of these forcings, including their absence, to allow isolation of individual wave, tide and WTI components. King et al., (2019) derived a classification scheme for categorising the dominant sand transport mode between wave, tide and WTI dominance of sand transport (Section 2.2). From these simulations, it is possible to extract sand transport dominance class, net sand transport magnitude and the corresponding environmental variables for use in a predictive model.

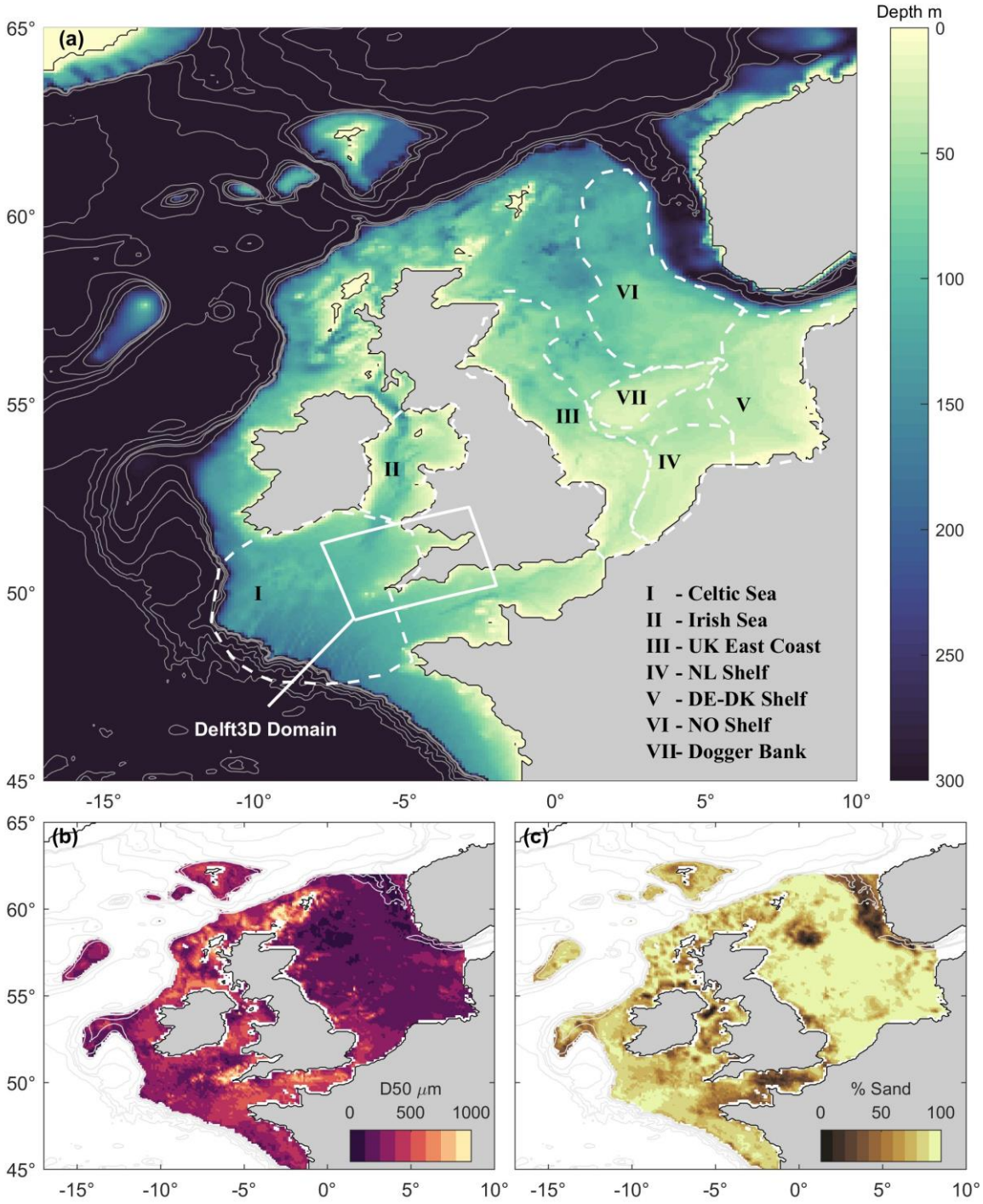

Figure 1: Maps of (a) depth, (b) median sand fraction grain size and (c) sand as a percentage of available sediment for the Northwest European Continental Shelf. Depths are taken from the FOAM-AMM7 model, whilst sediment characteristics are taken from Wilson et al. (2018). Selected shelf areas for later comparison are indicated and named in (a). The extent of the model domain of King et al. (2019) is also indicated.

158

159

2.2. Classification scheme

The classification scheme of King et al. (2019) categorises sand transport between wave-dominated, tide-dominated and non-linear-dominated, where non-linear refers to non-linear WTI (Figure 2). Classes are determined by two ratios:

$$R1 = T:(W + NL) = T:(WT - T), \quad (1)$$

$$R2 = W:NL \quad (2)$$

Where *R*1 represents the ratio of tide-only net sand transport magnitude (*T*) to the combined wave-only net transport magnitude (*W*) and the component attributed to non-linear WTI (*NL*). This determines the relative influence of waves (including non-linear interactions) versus tides, determined by subtracting the tidal component from the combined wave+tide net transport magnitude (*WT*). Ratio *R*2 represents the relative contribution on non-linear interactions versus waves alone. This allows the contribution of tides, waves and wave-tide interactions to be quantified, visualised and compared. This classification scheme considers net sand transport per tidal cycle, and the class can change under different combinations of wave and tidal forcing. Classification changes under different conditions qualitatively matched modelled shifts in sand transport direction (King et al., 2019; Pattiaratchi & Collins, 1988), supporting the predicted shift in the dominant mode of net sand transport.

This classification scheme results in three dominant modes of net sand transport (wave-dominated, W, tide dominated, T, and non-linear dominated, NL), where the respective forcing is responsible for at least 75% of the net sand transport magnitude. When the dominant class is responsible for >50% of net sand transport, but <75%, a subdominant class is defined (noted using lowercase letters). At present, this scheme requires results from coupled and uncoupled numerical simulations of net sand transport to calculate. The following section will examine kNN as a classification prediction method, based on defined predictor variables, which we will apply to this classification scheme (Section 2.3).

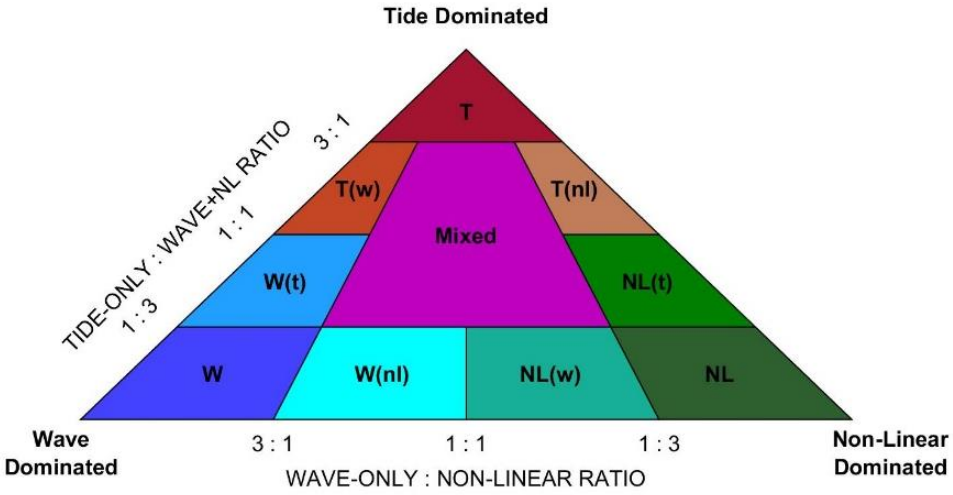

Figure 2: Classification scheme for sand transport dominant forcing proposed by King et al. (2019).

2.3. K-Nearest Neighbour (kNN)

Machine learning algorithms are being increasingly used in the geosciences (Lary et al., 2016; Kanevski et al., 2009). The kNN algorithm has been employed for prediction of seafloor properties in the geosciences including seafloor total organic carbon (Lee et al., 2019), isochore thickness (Lee et al., 2020) and sediment accumulation rates (Restreppo et al., 2020). Other applications of machine learning algorithms in the geosciences include predictions of seafloor sediment porosity (Martin et al., 2015) and seafloor fluid expulsion anomalies (Phrampus et al., 2019). The kNN algorithm is one of the simplest machine learning algorithms, and can be used in geospatial classification prediction (Kanevski et al., 2009). The algorithm works on the principle that areas with similar conditions are likely to share the same class.

The kNN algorithm requires a predictand (the variable or class we want to predict) and a set of defined predictors (variables we have measured or estimated). The algorithm is trained on the predictor data associated with known values of the predictand. The algorithm is then used to predict unseen data where the predictand is unknown by calculating the distance to the "k" nearest neighbours in parameter space to the new data, where "k" is the number of nearest points the algorithm uses for its calculation. The implementation used in this study is included in the MATLAB Statistics and Machine Learning Toolbox (MathWorks, 2020). The predicted class is the class with the minimum estimated cost, determined as a function of the probability that the new data comes from a particular class and the expected cost of misclassification for each observation. Numerous search methods exist for determining the nearest neighbours for use in the algorithm. In this study a *K*d-tree is used to perform

the nearest neighbour search, saving computation time as only a subset of the distances to points need to be calculated. Distances were calculated using a city-block distance metric with k = 7, as this provided optimal accuracy whilst minimising the value of k to avoid smoothing the data.

Model performance was determined using five-fold cross-validation of the training dataset. This entails splitting the dataset into five equal parts, and iteratively training the model on four of five parts, whilst validating using the fifth part by calculating the percentage of observations which were classified correctly, changing the validation fifth each time. The final model accuracy is an average of the five cross-validation scores. This method mitigates the likelihood of overfitting (Kanevski et al., 2009; Lee et al., 2019).

The choice of predictors is motivated by data availability, physical relevance to the prediction of net sand transport forcing mode and magnitude, as well as predictive value of each potential predictor. To assess the value of individual predictors, each predictor was tested in isolation to predict the class and order of magnitude of the net sand transport. The accuracy of each predictor was then compared with the predictive accuracy of an array of random numbers, to test whether predictors had greater predictive value than random noise. The selection of predictors, including their predictive accuracy, is described below (Section 2.4).

2.4. Environmental Predictors

Environmental predictors across the NW European Shelf used in this study are shown in Table 1a, including their sources and resolution (spatial, temporal) where applicable. Selection criteria were data availability, spatio-temporal resolution and predictive value. With these data sources defined, the model scenarios conducted to generate training data are included in Table 1b, including the range of the parameters used. Modelled scenarios were conducted as described in King et al. (2019), calculating net sand transport for wave-only, tide-only and wave+tide forcing over springs and neaps at 1-km resolution for an approx. 350 x 240 km region of the Celtic shelf with variable wave exposure and meso-megatidal regime. A full model description and validation is also presented therein. Additional scenarios were conducted in addition to those described in King et al. (2019) to include more intermediate wave conditions and a range of grain sizes. Mixed size fractions (e.g., sand-gravel mixtures) were not considered, and this is discussed in section 4.2. Dominant transport classes were calculated as in Figure 2, and order of magnitude of net sand transport was determined from the coupled wave+tide simulations. Predictors for training were determined from the uncoupled simulations to ensure WTI were not included in the predictor variables, replicating the uncoupled nature of the shelf-scale models.

Table 1

(a) Environmental predictors across the NW European Shelf; (b) Environmental predictors and scenarios used in Delft3D simulations to generate training data.

(a) Environmental predictors across the NW European Shelf

Predictor Name	Symbol	Units	Source	Spatial resolution	Temporal Resolution	Interpolation	Processing
Significant wave height	H_s	m	Tonani & Saulter (2020)	1.5 km	1 hour	Interpolated to 7km grid	Mean H_s per tidal cycle
Peak period	T_p	s	As H_s	1.5 km	1 hour	Interpolated to 7km grid	Mean T_p per tidal cycle
Power	P	W	As H_s	1.5 km	1 hour	Interpolated to 7km grid	Mean P per tidal cycle
Depth[+]	h	m	O'Dea et al. (2012)	7 km	-	Converted to MSL2000	-
Relative wave height	H_s/h	-	As H_s and h	7km	1 hour	-	Mean Hs/h per tidal cycle
Tide range	TR	m	Graham et al. (2018); O'Dea et al. (2012)	7 km	1 hour	-	Determined per tidal cycle
Max tidal current	U_{max}	ms^{-1}	As TR	7 km	1 hour	-	Determined per tidal cycle
Angle between waves and currents	ϑ	Deg	As H_s and TR	7 km	1 hour	-	Mean wave direction and max tidal current direction
Median grain size	D_{50}	µm	Wilson et al. (2018)	0.125°	-	Interpolated to 7km grid	-

(b) Modelled scenarios for training

Scenario	$H_s \cap T_p$ joint exceedance probability	H_s min, median, max (m)	T_p min, median, max (s)	Tide condition	TR min, median, max (m)	U_{max} min, median, max (ms^{-1})	D_{50} (µm)	Nº data
1	1%	0.2, 7.1, 8.5	5.9, 17.6, 19.0	Springs	1.8, 3.0, 7.8	0.03, 0.7, 3.6	125	44861
2*	1%	0.2, 7.1, 8.5	5.9, 17.6, 19.0	Springs	1.8, 3.0, 7.8	0.03, 0.7, 3.6	330	44683
3	1%	0.2, 7.1, 8.5	5.9, 17.6, 19.0	Springs	1.8, 3.0, 7.8	0.03, 0.7, 3.6	750	43582
4	1%	0.2, 7.1, 8.5	5.9, 17.6, 19.0	Neaps	0.6, 1.2, 4.2	0.02, 0.3, 1.5	125	44566
5*	1%	0.2, 7.1, 8.5	5.9, 17.6, 19.0	Neaps	0.6, 1.2, 4.2	0.02, 0.3, 1.5	330	43652
6	1%	0.2, 7.1, 8.5	5.9, 17.6, 19.0	Neaps	0.6, 1.2, 4.2	0.02, 0.3, 1.5	750	39972
7	10%	0.1, 4.1, 4.8	5.0, 14.9, 15.4	Springs	1.8, 3.0, 7.8	0.03, 0.7, 3.6	125	44577
8	10%	0.1, 4.1, 4.8	5.0, 14.9, 15.4	Springs	1.8, 3.0, 7.8	0.03, 0.7, 3.6	330	44272
9	10%	0.1, 4.1, 4.8	5.0, 14.9, 15.4	Springs	1.8, 3.0, 7.8	0.03, 0.7, 3.6	750	41709
10	10%	0.1, 4.1, 4.8	5.0, 14.9, 15.4	Neaps	0.6, 1.2, 4.2	0.02, 0.3, 1.5	125	41885
11	10%	0.1, 4.1, 4.8	5.0, 14.9, 15.4	Neaps	0.6, 1.2, 4.2	0.02, 0.3, 1.5	330	39175
12	10%	0.1, 4.1, 4.8	5.0, 14.9, 15.4	Neaps	0.6, 1.2, 4.2	0.02, 0.3, 1.5	750	16637
13	50%	0.1, 1.9, 2.1	3.4,10.5,10.8	Springs	1.8, 3.0, 7.8	0.03, 0.7, 3.6	125	43380
14*	50%	0.1, 1.9, 2.1	3.4,10.5,10.8	Springs	1.8, 3.0, 7.8	0.03, 0.7, 3.6	330	41224
15	50%	0.1, 1.9, 2.1	3.4,10.5,10.8	Springs	1.8, 3.0, 7.8	0.03, 0.7, 3.6	750	30842
16	50%	0.1, 1.9, 2.1	3.4,10.5,10.8	Neaps	0.6, 1.2, 4.2	0.02, 0.3, 1.5	125	13415
17*	50%	0.1, 1.9, 2.1	3.4,10.5,10.8	Neaps	0.6, 1.2, 4.2	0.02, 0.3, 1.5	330	10274
18	50%	0.1, 1.9, 2.1	3.4,10.5,10.8	Neaps	0.6, 1.2, 4.2	0.02, 0.3, 1.5	750	5265
Summary:	**1% – 50%**	**0.1 – 8.5**	**3.4 – 19.0**	**Springs – Neaps**	**0.6 – 7.8**	**0.02 – 3.6**	**125 – 750**	**633972**

Note: [+] Depth used as a predictor combined in H_s/h.

* Scenarios described in King et al. (2019).

An example of the relationship between tide range *TR*, maximum tidal current speed U_{max}, relative wave height H_s/h and the sand transport dominance classes of King et al. (2019) is shown in Figure 3. The modelled *TR* and U_{max} are shown as a function of H_s/h with class indicated by colour (Figure 3a, b). Tide-dominated areas exhibit low wave heights and stronger tidal currents and a greater tidal range, whilst wave-dominated areas are the inverse. Non-linear dominated areas occupy the mixed energy section of the parameter space. A three-predictor kNN classifier is shown in Figure 3c, indicating the classification boundaries for relative to the three predictors: new data falling within this parameter space will be classified accordingly. This is a simplified classifier for 3D visualisation, whereas the final classifier has eight dimensions (see Table 2).

Each of the eight predictors in Table 1 was tested in isolation and compared with classifications predicted by an array of random numbers to determine its predictive value. For a predictor to be accepted, it needed to have an accuracy greater than that of the random array, as in Lee et al. (2019). The predictive accuracy of each predictor is shown in Table 2 for the dominance class and order of magnitude. The only variable with a lower predictive value than random noise in isolation was median grain size D_{50} (test 9). To further test D_{50}, accuracy of the k-NN prediction was tested alongside the other predictors with and without D_{50} (tests 10 and 12) and also with and without the random array (tests 10 and 11). It was found that in conjunction with the other predictors, D_{50} provided a greater improvement in accuracy (class - 21.1%, magnitude - 46.3%) than the random array (class - 12.3%, magnitude - 9.1%), and was vital for an accurate prediction of the dominant class and order of magnitude (Table 2), therefore D_{50} was included as a predictor. Final predictive accuracy was 81.9% for class and 90.8% for magnitude, and most misclassified data were only out by one class.

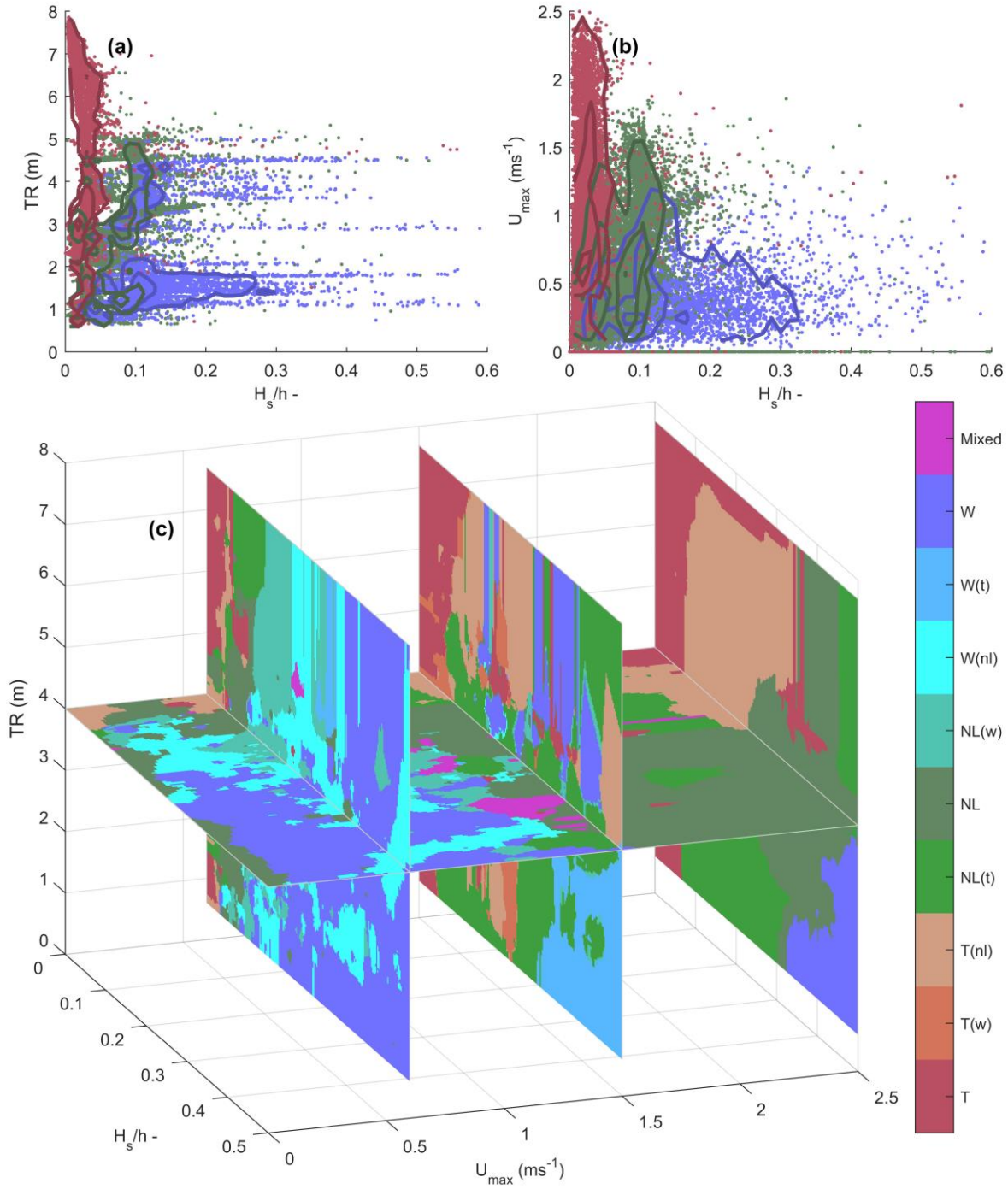

Figure 3: Relation of classes to predictor variables: (a, b) Modelled tide range *TR* and maximum tidal current speed U_{max} as a function of relative wave height H_s/h, data are coloured as per their associated dominance class (King et al., 2019), contours are shown to indicate point density for each class. Only data in the three primary classes are shown for simplicity (tide-dominated, wave-dominate and non-linear-dominated); (c) Example of classification boundaries for a simple 3D k-NN classifier using tide range, maximum current speed and relative wave height. New data falling within the 3D parameter space are classified accordingly. The actual classifier has 8 dimensions, and this should be viewed as a simplified example only.

258

Table 2

(a) Predictive accuracy of environmental predictors compared with calculated dominance classes and order of magnitudes from model data. Accuracy is determined from 5-fold cross-validation of the training dataset, and is calculated for a random number array (test 1), individual predictors (tests 2 – 9), and the combined predictors to further test D_{50} (tests 10 – 12). The accuracy of the final kNN prediction with all predictors is shown (test 12).

Test Number	Variable(s)	Symbol	Accuracy: Dominant class (King et al., 2019) % correct	Accuracy: Order of magnitude (OOM) % correct	Difference relative to random array for Class %	Difference relative to random array for OOM %
1	**Random array**	***Rnd***	**30.2**	**27.2**	-	-
2	Significant wave height	H_s	58.3	42.3	+28.1	+15.1
3	Peak period	T_p	49.2	27.4	+19.0	+0.2
4	Power	P	58.5	42.3	+28.3	+15.1
5	Relative wave height	H_s/h	58.2	42.1	+28.0	+14.9
6	Tide range	TR	49.1	28.7	+18.9	+1.5
7	Max tidal current	U_{max}	49.0	28.7	+18.8	+1.5
8	Angle between waves and currents	ϑ	43.0	35.1	+12.8	+7.9
9	Median grain size	D_{50}	9.4	24.5	-20.8	-2.7
10	All – D_{50} and Rnd	-	60.8	44.5	+30.6	+17.3
11	As 10 + Rnd	-	73.1	53.6	+42.9 (+12.3)*	+26.4 (+9.1)*
12[+]	**As 10 + D_{50}**	**-**	**81.9**	**90.8**	**+51.7 (+21.1)***	**+63.6 (+46.3)***

*Difference relative to test number 10.

[+]Test 12 represents the accuracy of the final kNN model used.

Tidal predictors (tide range *TR*, maximum current speed U_{max}) are shown across the NW European shelf in Figure 4a-d for springs and neaps. A distribution of *TR* over a statistically representative year is shown in Figure 4e-f at two locations marked with triangles in subplots a-b. The distribution of *TR* was calculated across each node the NW European shelf area over 1 year. Areas below the shelf break were excluded from analysis as they were below the maximum depth in the training data. Similarly, wave predictors are shown in Figure 5a-d. These predictors are shown for 1% and 50% joint exceedance of H_s and T_p, as determined from a fitted joint probability gumbel copula distribution (Genest & Favre, 2007) at each node across the domain over 1 year, using generalised extreme value and gamma marginal distributions for H_s and T_p respectively. Wave direction was taken as the mean wave direction over the year. Wave heights are in agreement with wave conditions for similar exceedances modelled by Bricheno et al. (2015). Depth was taken from the AMM7 model for calculation of H_s/h, whilst grain size was determined from the synthetic map created by Wilson et al. (2018; Figure 1). All variables were resampled where necessary to the AMM7 model grid at 7km resolution. The fitted distributions of tide range (e.g., Figure 4e, f) and joint H_s and T_p (e.g. Figure 5e, f) enable the generation of tide and wave forcing data for a statistically representative year, assuming wave and tide condition are independent, keeping water depth and grain size constant and using the

276 mean wave direction and maximum tidal current direction as an indicator of the direction difference
277 between waves and the tidal major axis.

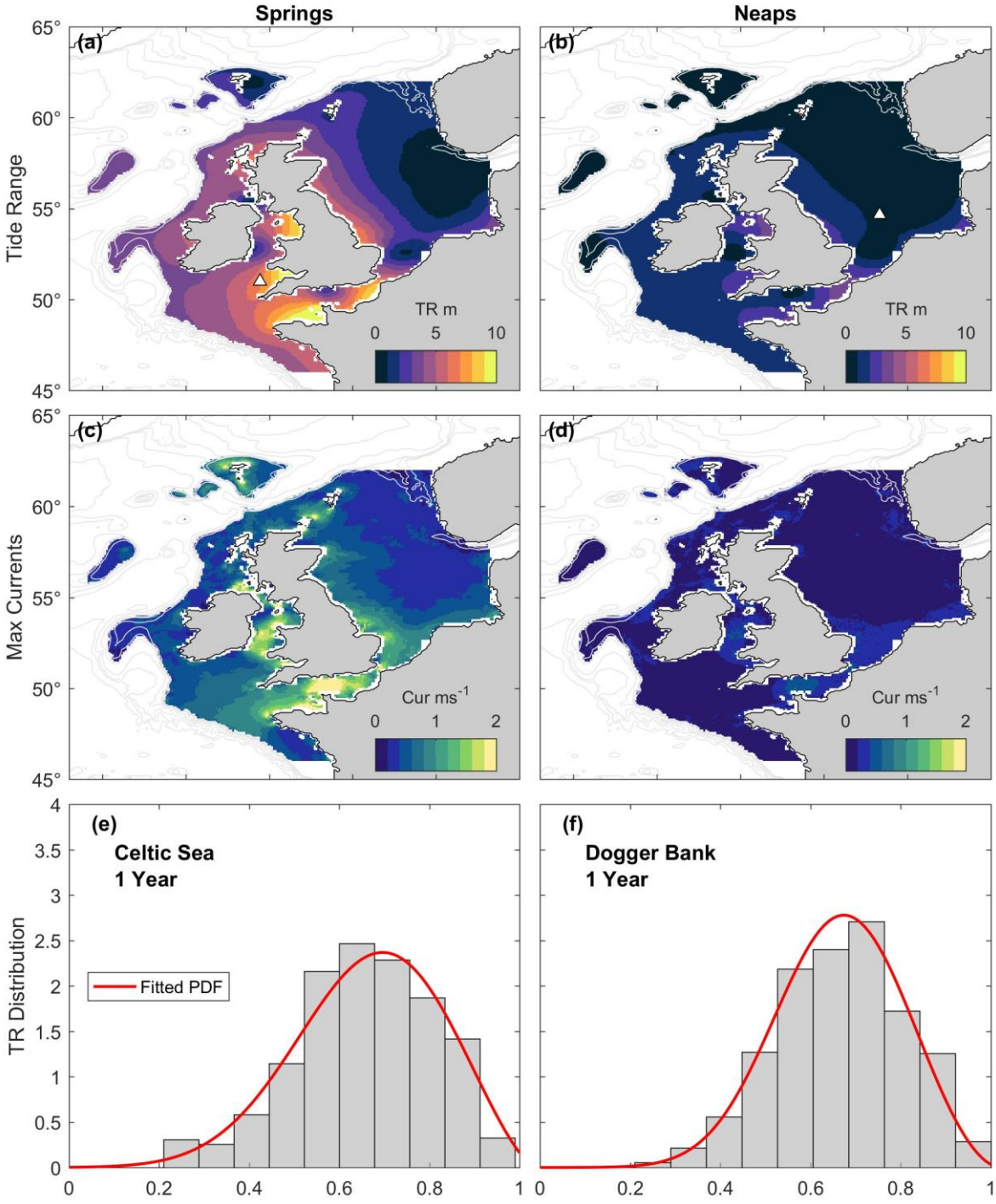

Figure 4: Maps of representative tide conditions across the NW European Shelf. Histograms show distributions of tide range (*TR*) normalised by the maximum tide range over 1 year for two locations indicated by white triangles in subplots (a) and (b) for their respective columns. Fitted probability distribution functions are shown (red curves).

278

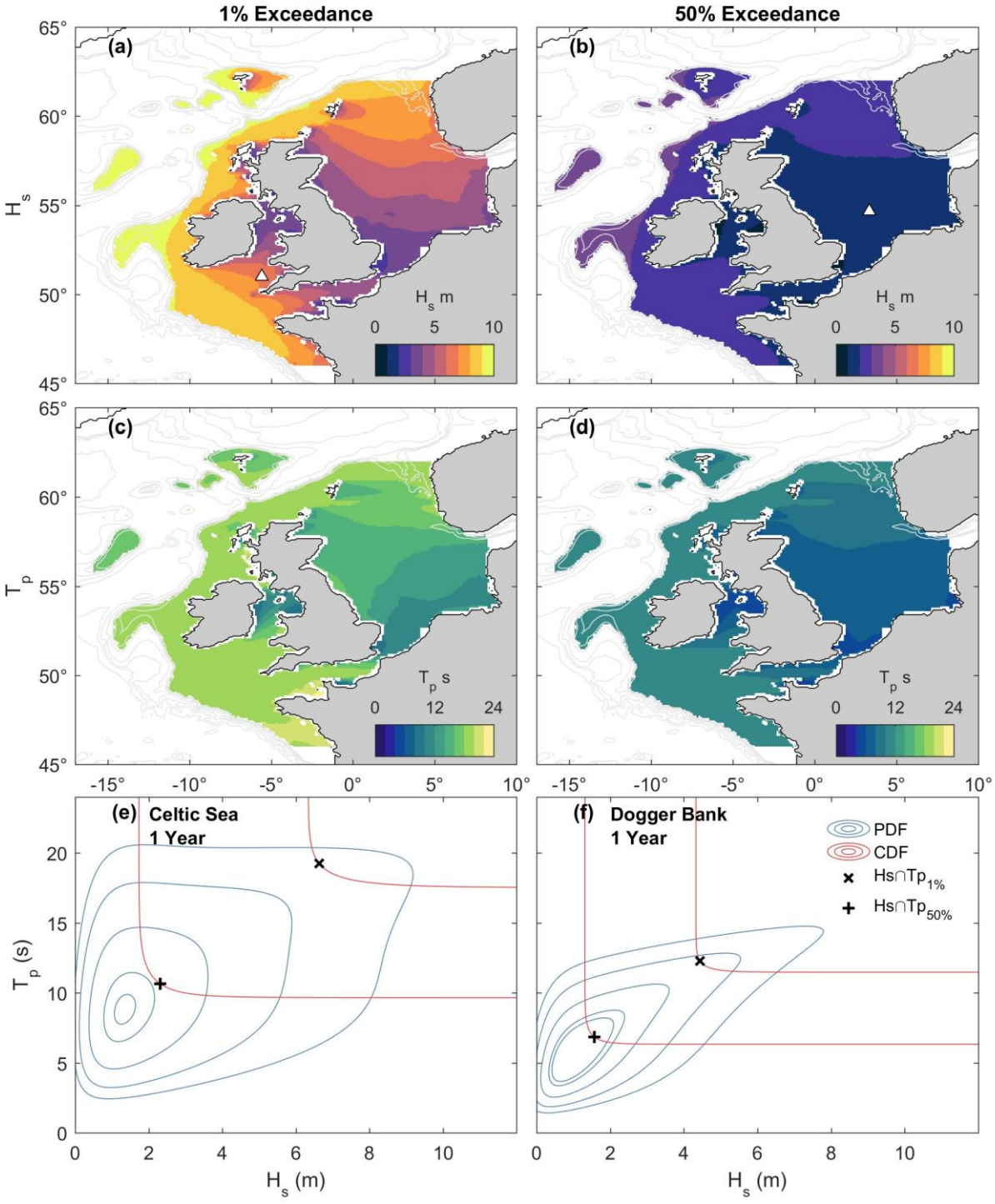

Figure 5: Maps of representative wave statistics (significant wave height H_s and peak period T_p), with joint probability distribution function (blue) and cumulative distribution function (red) contours for two locations over 1 year. Selected H_s and T_p for the 1% and 50% exceedance probability are indicated. The locations used for subplots € and (f) are indicated by white triangles in subplots (a) and (b) respectively.

279

280

3. Results

In this section we present the results of the kNN classification across the NW European shelf for different environmental conditions, and examine the influence of different conditions on the shelf areas presented in Figure 1a. We go on to present the determination of the dominant sand transport class and order of magnitude over a statistically representative year.

3.1. Environmental forcing controls on sand transport across the shelf

Results from the kNN prediction for different environmental forcing conditions are presented as maps in Figure 6. The dominant class, indicating the dominant driver of sand transport, and the potential order of magnitude of net sand transport are presented for spring (Figure 6a,b,e,f) and neap (Figure 6c,d,g,h) tides under median (50% exceedance; Figure 6a,b,c,d) and extreme (1% exceedance; Figure 6e,f,g,h) wave forcing as characterised for each node on the shelf area (see Figures 4 & 5). Regions greater than 140 metres depth are excluded to avoid extrapolation, as these exceed the largest depth in the training model and are deep enough that wave impacts are likely to be minimal.

Coastal areas around the UK are generally tide-dominated at spring tides and median wave forcing, with the second largest predicted order of magnitude of potential net sand transport (Figure 6a, b), exceeded only by the extreme waves at spring tide conditions (Figure6e, f). This includes large areas of the meso-macrotidal Celtic shelf, UK East Coast and the Irish Sea. Deeper areas of the shelf tended to show dominance of non-linear interactions, with net transport several orders of magnitude lower. Only microtidal, shallow, wave-exposed areas such as Dogger Bank and the DE-DK Shelf show wave-dominance in these conditions. The lowest magnitudes are found for median waves at neaps, where only the shallow, exposed areas of the NL and DE-DK Shelves show elevated net sand transport driven by waves (Figure6c, d). Sand transport is effectively switched off for most other shelf areas under these low energy conditions.

In the highest energy conditions with extreme waves at springs, macro-meso tidal areas show dominance of WTI, whilst waves dominate sand transport in the Eastern North Sea where tidal currents are weaker (Figure 6e, f). Sand transport is dominated by waves across this shelf area during extreme waves at neaps, with the greatest magnitudes in finer grained, shallow and wave exposed areas of the NL and DE-DK Shelves in the Eastern North Sea (Figure 6g, h). This is despite these areas having lower wave energy at this exceedance than more swell exposed regions (e.g., Celtic Shelf), indicating the importance of grain-size and water depth as controls. The next section explores the influence of environmental forcing conditions in more detail for the different shelf areas.

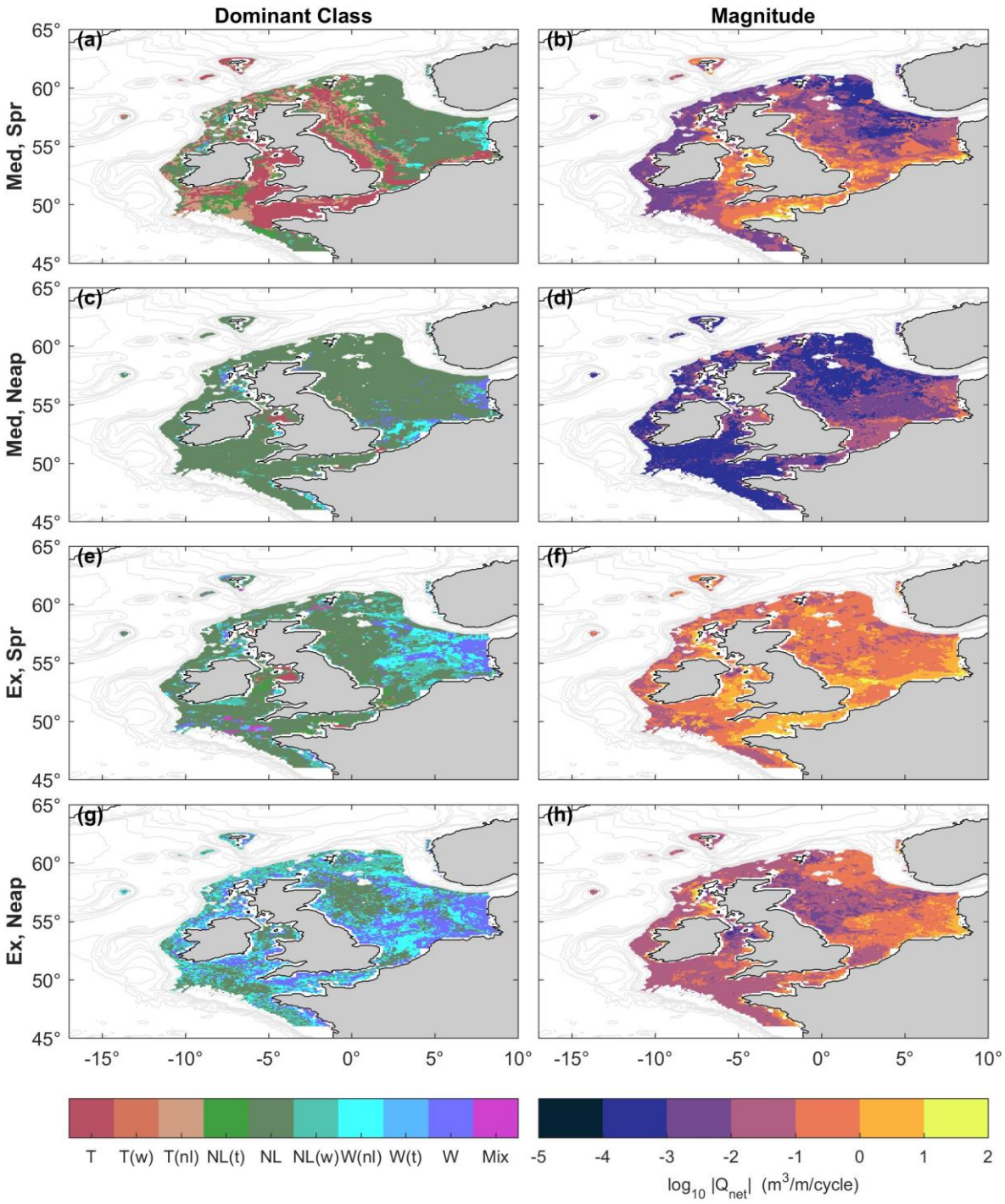

Figure 6: Results from the KNN predictions for different conditions presented as maps, including dominant transport mode classification (left column) and order of magnitude (right column). Colours on the right column are on a logarithmic scale. Extreme (1% exceedance; Ex) and median (50% exceedance; Med) wave forcing is shown at springs (Spr) and neaps (Neap).

313

3.2. Environmental forcing controls on sand transport for shelf sub-areas

A sensitivity analysis for different shelf areas was conducted by changing the environmental forcing conditions, including tidal condition, wave exceedance and grain size, and calculating the average class across each shelf area. To determine an average class, the kNN-predicted classification for each node within the designated region (Figure 1a) was converted to a representative pair of ratios R1 and R2 (Equations 1 & 2; Figure 2). Values of R1 and R2 were taken as the centre value of each classification bin, whilst end values (e.g., for R1 > 3 in tide-dominated conditions) were assumed to be dominant by a factor 6 in their respective direction (e.g., R1 = 6 for tide-dominated transport). The mean R1 and R2 of all nodes within each region was calculated, weighted by the predicted net transport magnitude. These results are presented in Figure 7.

The same wave and tidal forcing conditions are presented as shown in Figure 6. Symbols are placed within the classification triangle according to the regional mean R1 and R2 for that forcing condition. The influence of grain size variation is shown in Figure 7b. This is an indication of the variability in the response throughout the region arising from the spatial variability of grain size (D_{50}). The dominant class was calculated for the median, 2.5th and 97.5th centiles of D_{50} through each region. Sand transport was more tidally dominated for finer grain sizes, due to easier resuspension. For clarity, the results for the other regions are shown for the median D_{50} through that region, with an indication of the variability in grain size shown on a scale.

Environmental forcing conditions are the primary control on the dominant net sand transport mode, with grain size moderating this. Different shelf areas exhibit different responses to changing forcing. Most shelf areas are tidally dominated for median wave forcing at spring tides, with the exception of Dogger Bank and the microtidal area of the NO Shelf considered in this study, which have very low tidal sand transport magnitudes (Figure6b) and are classified as non-linear dominated. Under median waves at neaps, tidal sand transport is low across the shelf and non-linear interactions drive the sand transport that does occur. For extreme waves at springs, sand transport in all areas is dominated by WTI, whereas at neaps, shallower, finer grained and mesotidal areas such as the UK East Coast, Dogger Bank and the DE-DK Shelf shift to wave dominated sand transport. The macrotidal Celtic sea remains non-linear dominated in these conditions, as well as the relatively sheltered Irish Sea, although tending towards greater wave-dominance than at springs. The next step is to determine which forces drive net sand transport over a statistically representative year, and the order of magnitude of that sand transport, taking the full annual distribution of waves and tides into account.

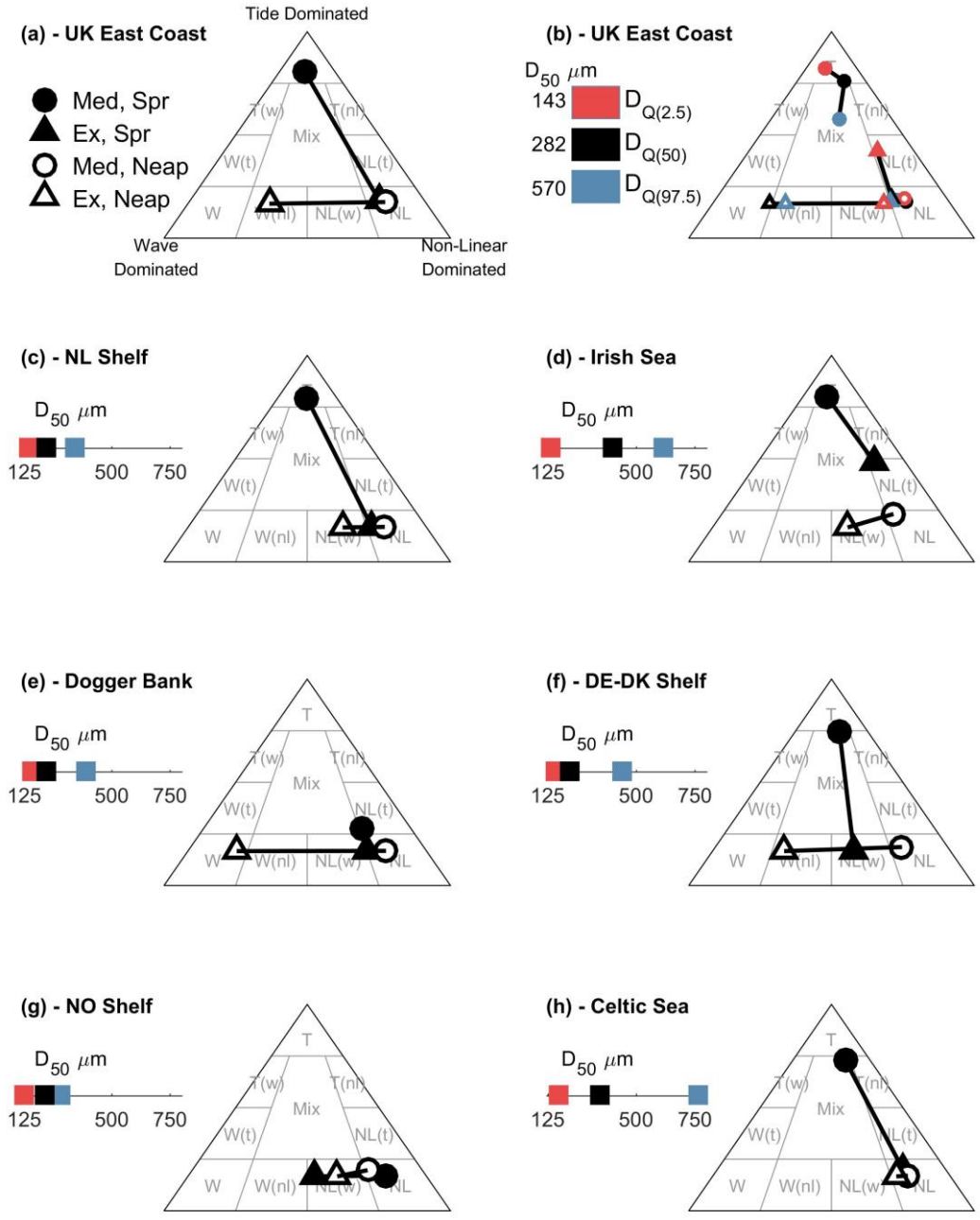

Figure 7: Sensitivity analysis for different shelf areas under changing environmental forcing conditions. "Ex" denotes 1% exceedance "Extreme" wave forcing, "Med" denotes 50% exceedance "Median" wave forcing. $D_{Q(N)}$ denotes the Nth quantile of the sediment D_{50} diameter as distributed through the specified region. (b) The influence of grain size on the predicted classification for the UK East Coast region. Red and blue symbols indicate the class for the 2.5th and 97.5th centiles D_{50} in the region, respectively. Other shelf areas show the class for the median D_{50} in these regions. The 2.5th, 50th and 97.5th centile D_{50} values are indicated on linear scales next to the classification triangle for each region.

345

3.3. Dominance and magnitude of net sand transport over a year

Using the fitted tide range distribution (e.g. Figure 4e, f), and the fitted copula joint probability distribution for significant wave height and peak period (e.g. Figure 5e, f) for each node across the shelf, it was possible to generate tide and wave forcing data for a statistically representative year of semi-diurnal tidal cycles. By assuming independence between wave condition and tide condition, keeping water depth and grain size constant, and using the mean wave direction and tidal maximum current direction, it was possible to tabulate a representative set of predictors over a statistically representative year. These were then used to determine a classification and order of magnitude for each tidal cycle. The sum of the order of magnitude over the statistically representative year gives a sense of the magnitude of potential net sand transport across the shelf over one year, whilst the classification for each node was determined as the class for which the maximum net sand transport occurred over the year. Results are shown in Figure 8.

Net sand transport ranges from approx. 10 $m^3m^{-1}y^{-1}$ in deeper, microtidal areas of the NO Shelf, to up to 10000 $m^3m^{-1}y^{-1}$ in more wave exposed areas of the DE-DK Shelf and the macrotidal areas of the south west English Channel. Much of the shelf surrounding the UK is tidally dominated, whilst deeper areas of the shelf, including much of the Celtic Sea and NO Shelf, are dominated by non-linear WTI. Shallow, fine grained areas of Dogger Bank and the DE-DK shelf are dominated by wave driven sand-transport, reflecting the lower tidal velocities across these regions. The NL Shelf is also dominated by non-linear WTI, reflecting stronger tidal currents and coarser grain size than Dogger Bank and the DE-DK Shelf (Figures 1b & 4). This does not consider wind driven net sand transport, nor the influence of sand-mud or sand-gravel mixtures. Areas with very low fractions of sand (Figure 1c) are included in these figures, and therefore these results should be considered potential net sand transport magnitude assuming continual availability of sand at the bed. These points are discussed in detail in section 4.2. In addition, a comparison to observed sand wave morphology is made in the Discussion (Section 4.1).

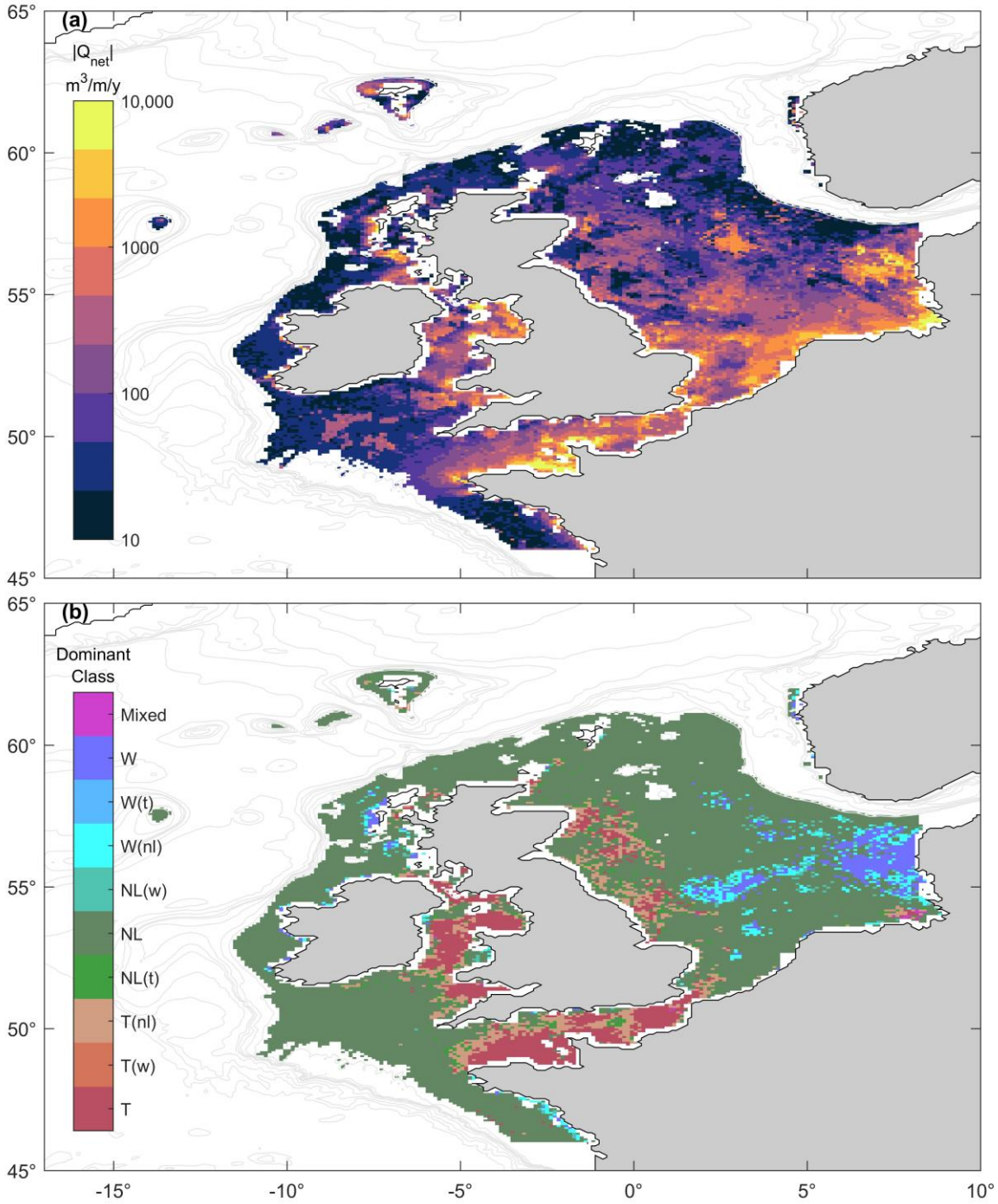

Figure 8: Dominant net sand transport classification and order of magnitude integrated over a statistically representative year using forcing conditions taken from the wave exceedance joint-probability distributions and tidal range probability distributions.

371

372

373

4. Discussion

The magnitude of net sand transport and relative dominance of waves, tides and their non-linear interactions was predicted for the Northwest European Continental Shelf using a kNN approach trained on extensive numerical modelling data on the Celtic Shelf area using a coupled hydrodynamic, wave and sand transport model (King et al., 2019). This shelf area has a highly varied tidal climate ranging from micro- to mega-tidal, varying degrees of wave exposure and a highly energetic wave climate (Harris & Coleman, 1998). These factors result in a varied parameter space with which to test the application of this kNN classification approach whilst generating insights into the dynamics of sand transport across this shelf.

The dominance of waves on the DE-DK Shelf and Dogger Bank, and dominance of tides along the UK East Coast predicted here is in agreement with modelling of wave, wind and tidal sand transport in the North Sea (van der Molen, 2002), lending confidence to the predictions of the kNN model. This paper builds upon previous work by considering the influence of WTI, indicating that non-linear wave-tide interaction dominates along the Dutch Shelf and deeper areas of the Celtic Sea and the Norwegian Shelf. This paper also presents a computationally efficient method for estimating the dominant processes influencing net sand transport, and its magnitude, for different environmental forcing conditions using readily available data. In the next section we examine a potential application of this method to look at the influence of environmental forcing parameters on sand wave morphology. We then discuss other applications, limitations and future work that arises from this.

4.1. Comparison with sand wave morphology

Modelling of sand wave dynamics is important for offshore renewable energy industrial activities and studies have been conducted to understand their dynamics in the Dutch North Sea and elsewhere (Cheng et al., 2020; Damen et al., 2018; Roetert et al., 2017; Van Oyen et al., 2011; van Santen et al., 2011; Wang et al., 2019). Tidal sand waves are also habitat to benthic species whose spatial distribution is dependent upon sand wave morphology, with feedback effects on sand wave evolution (Damveld et al., 2018; 2020).

Surface waves affect sand wave growth, wave length and migration, reducing sand wave height and increase wave length (Campmans et al., 2018a,b). Damen et al. (2018) examined sand waves on the NL Shelf, finding weaker than expected correlation of sand wave height with H_s possibly due to the interdependent and opposite acting correlations between H_s, water depth and sand wave height (Campmans et al., 2018a,b; Houthuys et al., 1994; Van Dijk & Kleinhans, 2005). They find that it is more reliable to consider the impact of the waves at the bed, for example using the Shields parameter.

406 Tidal currents are known to positively correlate with spatial frequency (Damen et al., 2018; Van
407 Santeen et al., 2011). Damen et al. (2018) find weak correlation between tidal currents and sand wave
408 height. It is important to consider the level of suspended sediment transport as a control on sand wave
409 length and height (Borsje et al., 2014; Damen et al., 2018). This could be a future application of this
410 kNN method, to predict the balance between suspended and bedload sand transport under variable
411 forcing conditions.

412 Here, we utilise same trained kNN classifier as presented earlier to predict the dominant transport
413 mode across the same region considered by Damen et al. (2018). Where possible, predictor data used
414 were taken from the dataset of Damen et al. (2017). These included 1% exceedance H_s, M2 current
415 amplitude (in lieu of the maximum tidal current) and grain size D_{50}. Tide range, current mean direction
416 and wave mean direction were interpolated from the shelf-scale predictors used earlier, and T_P was
417 interpolated from the 1% exceedance T_p (Figure 5c). The predicted transport class was determined at
418 1km resolution at the same locations as the data presented in Damen et al. (2018) and this is presented
419 in Figure 9a. Under these conditions we predict dominance of non-linear WTI in the southeast of the
420 sand wave field, moving to wave-dominance in the northwest.

421 The height, wave length and asymmetry of the sand waves was binned for each classification and
422 compared between classes (Figure 9b-d). This resulted in comparison of 9161 data points each
423 representing sand wave characteristics over a $1km^2$ area. Results suggest sand wave height is lowest
424 in wave dominated regions, and larger in regions dominated by non-linear WTI. Similarly, wave length
425 and asymmetry appear to increase with an increase in wave-dominance. The statistical dissimilarity of
426 the sand wave populations in each class was tested using the Kolmogorov-Smirnov (KS) test.
427 Distributions of sand wave characteristics were found to be unique between classes at the 95%
428 confidence level. A second one-sided KS test was performed to test the hypotheses that sand wave
429 height decreases moving from non-linear interaction dominated to wave dominated sand transport,
430 and that wave length and asymmetry increase. These hypotheses were found to be true at the 95%
431 confidence level, and P-values are included in Figure 9e-g.

432 These results are in agreement with previous research into wave and tidal influences on sand wave
433 height, wave length and asymmetry (Campmans et al., 2018a,b; Damen et al., 2018), lending
434 confidence to the results of the kNN prediction and indicating WTI may play a significant role
435 influencing sand wave morphology, and this classification scheme has a predictive power for sand
436 wave morphology on sandy continental shelves. This prediction is based on the most energetic wave
437 and tidal conditions. The annual classification determined in Figure 8 indicates this region is dominated
438 by non-linear WTI on an annual scale, suggesting that the more energetic conditions play a significant

role in controlling sand wave morphology, with increased wave-dominance under storm conditions limiting sand wave heights.

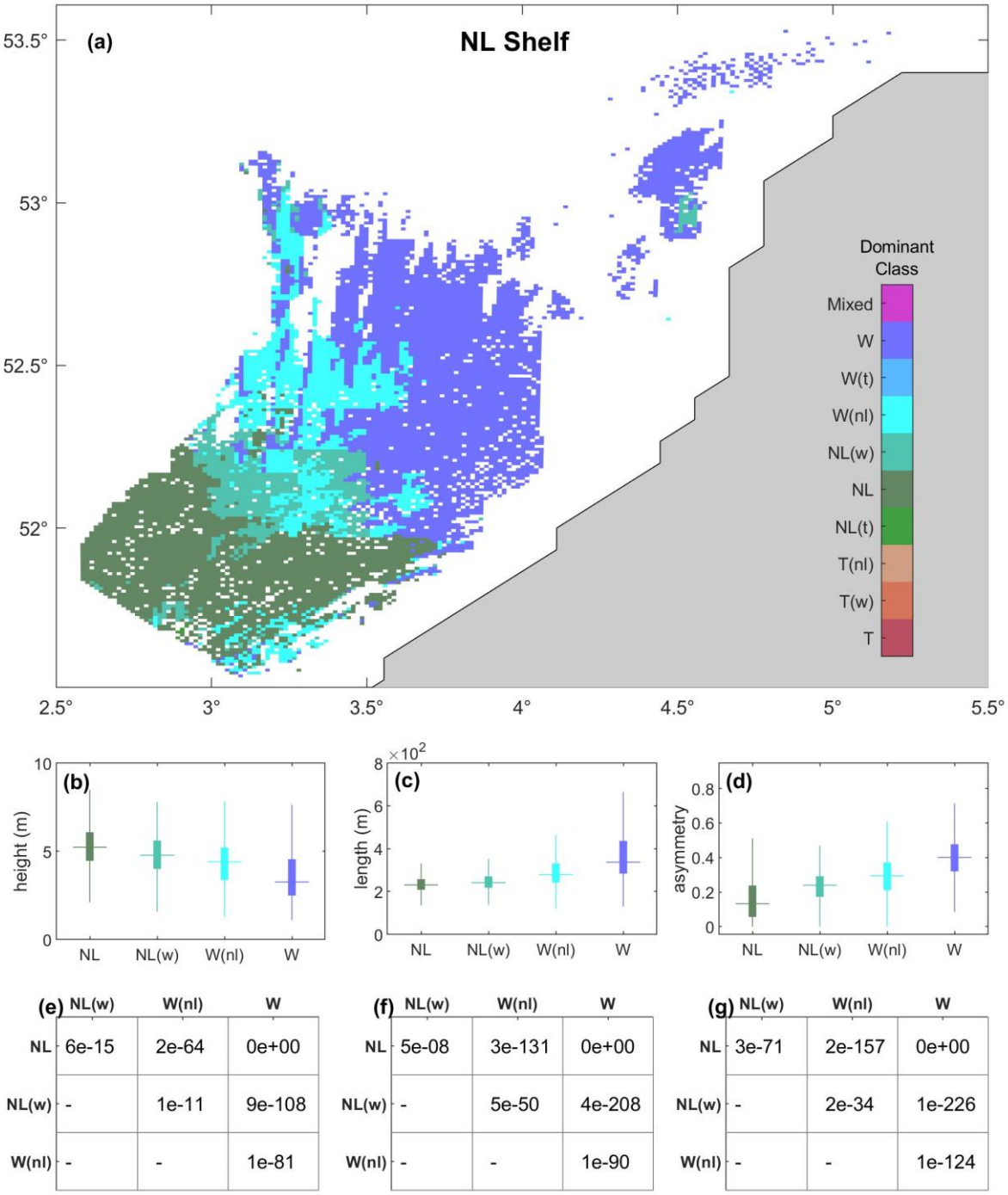

Figure 9: Application of classification prediction to sand wave physical characteristics averaged per square kilometre as per Damen et al. (2018). (a) Sand transport dominant class across the NL Shelf determined with a mix of environmental data from Damen et al. (2018) and other predictors as described earlier, interpolated to each square kilometre (1 pixel = 1 km^2). (b-d) Box plots showing

sand wave height, wave length and spatial frequency respectively for each dominant class. Plots indicate the median, 25th and 75th percentiles and whiskers indicate 1.5 times the IQR beyond the 75th or 25th percentile. (e-g) P-values from a 2-sample, 1-sided Kolmogorov-Smirnov test, testing if the data are significantly lower in magnitude in more wave dominated conditions (height, spatial frequency – e,g), or greater in magnitude in the more wave-dominated condition (wave length – f) at the 95% confidence level.

4.2. Assumptions, limitations and future work

In this study we show that the magnitude of net sand transport and the relative contribution from waves, tides and non-linear WTI is amenable to estimation using readily available wave and tidal data utilising a kNN classification prediction approach. The kNN method itself does not account for the physical relationships between predictors and the resultant classification, relying instead on the associations between predictors and classifications in the parameter space. This implies the trained classifier will only be representative of the physical processes represented in the training data. The trained classifier cannot therefore be used to extrapolate outside the range and physics represented in the data used to train it, however it can be applied in other regions. Here we discuss the processes represented in the model used to generate the training data, and the implications of those not represented.

Data used to train this kNN predictor were generated by a well validated numerical model of coupled hydrodynamics, waves and sand transport (King et al., 2019). The range of each predictor in the training data is shown in Table 1. Sand transport rates are determined using the formulation of van Rijn (2007a,b), therefore the predictor is representative of the physics included therein. Importantly, baroclinic and wind-driven currents are not included in the training model. This paper considers processes at the shelf scale, and due to the resolution of the forcing variables it should be considered to represent an estimate of the dominant sand transport processes on the continental shelf, and does not consider processes landward of the shoreface (approx. 15m) (e.g., Hamon-Kerivel et al., 2020; Héquette et al., 2008).

Important wind speed events can interact constructively or destructively with tidal currents to influence sand transport rates, depending on the relative angle of wind driven currents to the tidal current direction (Héquette et al., 2008). Wind driven currents are weak on the Celtic Shelf (Pingree & Le Cann, 1989), and wind driven residual currents across the NW European Shelf are likely to be most significant at neaps when tidal currents are weakest (Pingree & Griffiths, 1980), with the strongest wind driven residuals present in the Southern North Sea. Van der molen (2002) discusses wind driven sand transport relative to tides and wind waves in the Southern North Sea, finding wind-driven flows contribute significantly to net sand transport where tidal currents are small, alongside

wave driven currents. The areas defined by van der Molen (2002) as storm dominant (winds + waves) qualitatively agree with the wave dominated areas of the NL Shelf under energetic wave and tidal forcing presented in Figure 9. Their tide dominated area corresponds to the non-linear wave-tide interaction dominated part of the shelf, and it is noted that wave-tide interaction is not fully represented in their modelling. Whilst wind-driven circulations are beyond the scope of this study, this kNN method could be extended using a coupled training model to isolate the relative influence of wind-driven circulations on net sand transport and incorporate these into the classification.

Baroclinic circulations are not considered in this study either. Van Leeuwen et al. (2015) classify the North Sea by stratification regime. The regions of greatest net sand transport predicted here correspond qualitatively with areas either permanently mixed or intermittently stratified conditions, with seasonally stratified conditions affecting the deeper, microtidal areas of the North Sea which are predicted to have a lower magnitude of net sand transport. In winter, the NW European shelf area considered in this study is well mixed whilst areas such as the UK East Coast, the NL Shelf, the DE-DK Shelf and English Channel tend to remain well mixed or show weak stratification through spring, summer and autumn (Holt et al., 2010), and therefore baroclinic effects are not expected to influence significantly the prediction of this model in these regions.

An additional limitation is that this study only considers a pure sand bed, whereas sand-mud and sand-gravel mixtures affect sand resuspension (McCarron et al., 2019; Thompson et al., 2019). Graded sediment transport resulting from heterogeneous, bimodal sand distributions may also affect the wave length of sand waves (Van Oyen & Blondeaux, 2009). In sand-gravel mixtures, the hiding-exposure effect increases the critical shear stress required to mobilise the sand fraction, its effect becoming more significant for mixtures of >10% gravel (McCarron et al., 2019). Much of the North Sea sediment is comprised of > 90% sand (Figure 1c), and this effect is most likely to impact predictions on shelf areas with a higher coarse grain size fraction such as the Celtic Sea. Whilst we also do not consider biological effects on sediment resuspension, Thompson et al. (2019) show physical sediment characteristics to be more significant than biological factors in controlling bed stability. The purpose of this kNN classification method is to be applicable with readily available hydrodynamic and morphological data, therefore consideration of non-uniform grain size distributions, the effect of mixed sand-mud or sand-gravel substrates, and biological effects would necessarily add complexity to the predictive model and therefore limit its use by introducing a data requirement which may not be readily available to coastal practitioners. The method could be extended to include the effects of mixed grain size fractions in future.

The benefit of this method is to enable a rapid assessment of the dominant processes affecting net sand transport, and its magnitude, without the need for a computationally expensive numerical model. We show that the classification scheme of King et al. (2019) has predictive value for sand wave morphology on the NL Shelf, as a further application of this method. Whilst this paper considers shelf-scale processes, this classification scheme can be applied to other sand transport processes in the nearshore, such as headland bypassing (King et al, Under Review). The computational efficiency of this method relative to running a coupled wave-tide numerical model enables quick assessment to be made of the influence of changing environmental conditions such as upward trends in storminess across central, western and northern Europe (Castelle et al., 2018; Donal et al., 2011) on the magnitude and dominant forces driving the net transport of sand on sandy continental shelves, with potential applications globally.

5. Conclusions

In this paper we apply a data driven method to predict the dominant sand transport drivers and magnitude across a sandy continental shelf. We use k-Nearest Neighbour classification prediction trained with data from coupled hydrodynamic, wave and sediment transport modelling on a subdomain of the shelf to predict sand transport magnitude and mode across the entire shelf, using readily available wave, tide and morphological data. Key findings of this paper include:

- The relative dominance of waves, tides and non-linear wave-tide interactions (WTI) in the net transport of sand over a tidal cycle, as well as net sand transport magnitude, are amenable to prediction using readily available environmental predictors. These are: significant wave height, peak period, mean wave direction, wave power, tide range, maximum tidal current speed and direction, water depth and median grain size.
- Wave and tidal conditions are primary controls on net sand transport mode and magnitude, whilst grain size is a secondary control.
- Different shelf areas exhibit different dominant drivers of net sand transport for similar exceedance conditions, relating to differences in water depth, grain size, tide range and wave exposure between regions.
- Most shelf areas are tide-dominated for median waves at springs. For extreme waves at springs, most areas show dominance of WTI. At neaps, with median waves, sand transport is very low across the shelf, driven by wave-tide interaction where it does occur. Extreme waves at neaps result in wave-dominated sand transport in shallow or microtidal areas of the North Sea, as WTI dominated sand transport in deeper or macrotidal regions.

- Sand transport magnitude and dominance was predicted for a statistically representative year based on distributions of tide range and H_s-T_p joint-probability calculated across the shelf. Potential net sand transport shows tidal dominance in meso-macrotidal waters around the UK, wave-dominance on Dogger Bank and the German/ Denmark Shelf, and dominance of WTI on the Netherlands shelf and in deeper areas of the North Sea and Celtic Sea.
- The kNN prediction was applied at higher resolution to the Netherlands shelf area, and classes for energetic (conditions 1% exceedance waves at spring tide) compared with sand wave morphology across the region with data obtained from Damen et al. (2017). Sand wave height is shown to significantly (95% confidence) reduce with greater wave-dominance, while sand wave length and asymmetry significantly increase. Sand wave morphologic parameters were significantly different between predicted classes at the 95% confidence level.
- This paper presents a computationally efficient method to determine an initial estimate of the dominant driving forces and magnitude of net sand transport on sandy continental shelves, enabling efficient large-scale comparison between different regions and testing of the influence of changing environmental forcing on net sand transport with applications globally.

6. Acknowledgements

We acknowledge the UK Hydrographic Office for VORF corrections. We acknowledge the MET Office (Andy Saulter) for the hydrodynamic, bathymetric, and wave forcing data and NOAA for atmospheric pressure and wind data, and EMODnet bathymetry Consortium for the EMODnet Digital Bathymetry (DTM 2016). This research was supported by the NERC-funded BLUECoast Project (NE/N015525/1). Sand wave data used in this study are available at https://doi.org/10.4121/uuid:0d7e016d-2182-46ea-bc19-cdfda5c20308 and we thank Damen et al. (2017) for making this valuable dataset available. The other data on which this paper is based are publicly available from the corresponding author and will be made available online via the University of Plymouth PEARL open access research repository upon publication.

7. References

Aldridge, J. N., Parker, E. R., Bricheno, L. M., Green, S. L. & van der Molen, J. (2015). Assessment of the physical disturbance of the northern European Continental shelf seabed by waves and currents. *Continental Shelf Research*, 108, 121-140. https://doi.org/10.1016/j.csr.2015.03.004

Besio, G., Blondeaux, P., Brocchini, M., Hulscher, S. J. M. H., Idier, D., Knaapen, M. A. F., Németh, A. A., Roos, P. C. & Vittori, G. (2008). The morphodynamics of tidal sand waves: A model overview. *Coastal Engineering*, 55(7-8), 657-670. https://doi.org/10.1016/j.coastaleng.2007.11.004

Booij, N., Holthuijsen, L. H. & Ris, R. C. (1999). A third-generation wave model for coastal regions 1. Model description and validation. *Journal of Geophysical Research: Oceans*, 104(C4), 7649-7666. https://doi.org/10.1029/98JC02622

Borsje, B. W., Kranenburg, W. M., Roos, P. C., Matthieu, J. & Hulscher, S. J. M. H. (2014). The role of suspended load transport in the occurrence of tidal sand waves, *Journal of Geophysical Research: Earth Surface*, 119, 701–716. https://doi.org/10.1002/2013JF002828

Bricheno, L. M., Wolf, J., & Aldridge, J. (2015). Distribution of natural disturbance due to wave and tidal bed currents around the UK. *Continental Shelf Research*, 109, 67–77. https://doi.org/10.1016/j.csr.2015.09.013

Campmans, G. H. P., Roos, P. C., de Vriend, H. J., & Hulscher, S. J. M. H. (2018a). The influence of storms on sand wave evolution: A nonlinear idealized modeling approach. *Journal of Geophysical Research: Earth Surface*, 123, 2070– 2086. https://doi.org/10.1029/2018JF004616

Campmans, G. H. P., Roos, P. C., Schrijen, E. P. W. J., & Hulscher, S. J. M. H. (2018b). Modeling wave and wind climate effects on tidal sand wave dynamics: A North Sea case study. *Estuarine, Coastal and Shelf Science*, 213, 137– 147. https://doi.org/10.1016/j.ecss.2018.08.015

Carter L. & Heath R. A. (1975). Role of mean circulation, tides, and waves in the transport of bottom sediment on the New Zealand continental shelf. *New Zealand Journal of Marine and Freshwater Research*, 9:4, 423-448. https://doi.org/10.1080/00288330.1975.9515579

Castelle, B., Dodet, G., Masselink, G., & Scott, T. (2018). Increased winter-mean wave height, variability and periodicity in the North-East Atlantic over 1949–2017. *Geophysical Research Letters*, 45, 3586–3596. https://doi.org/10.1002/2017GL076884

Cieślikiewicz, W., Dudkowska, A., Gic-Grusza, G. & Jędrasik, J. (2018). Assessment of the potential for dredged material dispersal from dumping sites in the Gulf of Gdańsk. *Journal of Soils and Sediments* 18, 3437–3447. https://doi.org/10.1007/s11368-018-2066-4

Cheng, C. H., Soetaert, K., & Borsje, B. W. (2020). Sediment Characteristics over Asymmetrical Tidal Sand Waves in the Dutch North Sea. *Journal of Marine Science and Engineering*, 8(6), 409. https://doi.org/10.3390/jmse8060409

609 Collins, M. B. (1987). Sediment transport in the Bristol Channel: A review. Proceedings of the
610 Geologists' Association, 98(4), 367 – 383.
611 https://doi.org/10.1016/S0016-7878(87)80076-7

612 Damen, J. M., van Dijk, T. A. G. P., & Hulscher, S. J. M. H. (2017). Replication data for: Spatially
613 varying environmental properties controlling observed sand wave morphology. *4TU*.
614 https://doi.org/10.4121/uuid:0d7e016d-2182-46ea-bc19-cdfda5c20308

615 Damen, J. M., van Dijk, T. A. G. P., & Hulscher, S. J. M. H. (2018). Spatially Varying Environmental
616 Properties Controlling Observed Sand Wave Morphology. Journal of Geophysical Research:
617 Earth Surface, 123(2), 262–280.
618 https://doi.org/10.1002/2017JF004322

619 Damveld, J. H., van der Reijden, K. J., Cheng, C., Koop, L., Haaksma, L. R., Walsh, C. A. J., et al. (2018).
620 Video transects reveal that tidal sand waves affect the spatial distribution of benthic
621 organisms and sand ripples. *Geophysical Research Letters*, 45, 11,837– 11,846.
622 https://doi.org/10.1029/2018GL079858

623 Damveld, J. H., Borsje, B. W., Roos, P. & Hulscher, S. (2020). Biogeomorphology in the marine
624 landscape: modelling the feedbacks between patches of the polychaete worm Lanice
625 conchilega and tidal sand waves. *Earth Surface Processes and Landforms*, 45(11), 2572-2587.
626 https://doi.org/10.1002/esp.4914

627 Dernie, K. M., Kaiser, M. J. & Warwick, R. M. (2003). Recovery rates of benthic communities
628 following physical disturbance. *Journal of Animal Ecology*, 72(6), 1043-1056.
629 https://doi.org/10.1046/j.1365-2656.2003.00775.x

630 Donal, M. G., Renggli, D., Wild, S., Alexander, L. V., Leckebusch, G. C., & Ulbrich, U. (2011). Reanalysis
631 suggests long-term upward trends in European storminess since 1871. *Geophysical Research*
632 *Letters*, 38, L14703.
633 https://doi.org/10.1029/2011GL047995

634 Draper, L. (1967). Wave activity at the sea bed around northwestern Europe. *Marine Geology*, 5(2),
635 133 – 140.
636 https://doi.org/10.1016/0025-3227(67)90075-8

637 Fredsøe, J. (1984). Turbulent boundary layer in wave-current motion. *Journal of Hydraulic*
638 *Engineering*, 110(8), 1103–1120.
639 https://doi.org/10.1061/(ASCE)0733-9429(1984)110:8(1103

640 Genest, C., & Favre, A.-C. (2007). Everything you always wanted to know about copula modeling but
641 were afraid to ask. *Journal of Hydrologic Engineering*. 12(4), 347–368.
642 https://doi.org/10.1061/(ASCE)1084-0699(2007)12:4(347)

643 Graham, J. A., O'Dea, E., Holt, J., Polton, J., Hewitt, H. T., Furner, R., Guihou, K., Brereton, A., Arnold,
644 A., Wakelin, S., Castillo Sanchez, J. M., & Mayorga Adame, C. G. (2018). AMM15: a new high-
645 resolution NEMO configuration for operational simulation of the European north-west shelf.
646 *Geoscientific Model Development*, 11(2), 681–696.
647 https://doi.org/10.5194/gmd-11-681-2018

648 Grant, W. D., & Madsen, O. S. (1979). Combined wave and current interaction with a rough bottom.
649 *Journal of Geophysical Research*, 84(C4), 1797–1808.
650 https://doi.org/10.1029/JC084iC04p01797

Grant, W. D., & Madsen, O. S. (1986). The continental-shelf bottom boundary layer. *Annual Review of Fluid Mechanics*, 18(1), 265–305. https://doi.org/10.1146/annurev.fl.18.010186.0014

Hall, S.J. (1994) Physical disturbance and marine benthic communities: life in unconsolidated sediments. *Oceanography and Marine Biology: an Annual Review*, 32, 179–239.

Hansen, J. E., Elias, E., List, J. H., Erikson, L. H., & Barnard, P. L. (2013). Tidally influenced alongshore circulation at an inlet-adjacent shoreline. *Continental Shelf Research*, 56, 26–38. https://doi.org/10.1016/j.csr.2013.01.017

Hamon-Kerivel, K., Cooper, A., Jackson, D., Sedrati, M. & Pintado, E. G. (2020). Shoreface mesoscale morphodynamics: A review. *Earth Science Reviews*, 209, 103330. https://doi.org/10.1016/j.earscirev.2020.103330

Harris, P. T. (2014). Shelf and deep-sea sedimentary environments and physical benthic disturbance regimes: A review and synthesis. Marine Geology, 353, 169-184. https://doi.org/10.1016/j.margeo.2014.03.023

Harris, P. T. & Coleman, R. (1998). Estimating global shelf sediment mobility due to swell waves. *Marine Geology*, 150, 171-177. https://doi.org/10.1016/S0025-3227(98)00040-1

Harris, P. T. & Collins, M. B. (1991). Sand transport in the Bristol Channel: Bedload parting zone or mutually evasive transport pathways? *Marine Geology*, 101(1-4), 209–216. https://doi.org/10.1016/0025-3227(91)90072-C

Héquette, A., Hemdane, Y. & Anthony E. J. (2008). Sediment transport under wave and current combined flows on a tide-dominated shoreface, northern coast of France. *Marine Geology*, 249, 226-242. https://doi.org/10.1016/j.margeo.2007.12.003

Holt, J., Wakelin, S., Lowe, J. & Tinker, J. (2010). The potential impacts of climate change on the hydrography of the northwest European continental shelf. *Progress in Oceanography*, 86(3-4), 361-379. https://doi.org/10.1016/j.pocean.2010.05.003

Houthuys, R., Trentesaux, A., & De Wolf, P. (1994). Storm influences on a tidal sandbank's surface (Middelkerke Bank, southern North Sea). *Marine Geology*, 121(1–2), 23–41. https://doi.org/10.1016/0025-3227(94)90154-6

Hopkins, J., Elgar, S., & Raubenheimer, B. (2015). Observations and model simulations of wave-current interaction on the inner shelf. *Journal of Geophysical Research: Oceans*, 121, 198–208. https://doi.org/10.1002/2015JC010788

Kanevski, M., Pozdnukhov, A . & Timonin, V. (2009). *Machine Learning for Spatial Environmental Data: Theory, Applications, and Software*. Lausanne, Switzerland: EPFL Press.

Kemp, P. H., & Simmons, R. R. (1982). The interaction between waves and a turbulent current: Waves propagating with the current. *Journal of Fluid Mechanics*, 116, 227–250. https://doi.org/10.1017/S0022112082000445

Kemp, P. H., & Simmons, R. R. (1983). The interaction of waves and a turbulent current: Waves propagating against the current. *Journal of Fluid Mechanics*, 130(1), 73–89. https://doi.org/10.1017/S0022112083000981

King, E. V., Conley, D. C., Masselink, G., Leonardi, N., McCarroll, R. J., & Scott, T. (2019). The impact of waves and tides on residual sand transport on a sediment-poor, energetic, and macrotidal continental shelf. *Journal of Geophysical Research: Oceans*, 124, 4974– 5002. https://doi.org/10.1029/2018JC014861

King, E. V., Conley, D. C., Masselink, G., Leonardi, N., McCarroll, R. J., Scott, T., & Valiente, N. G. (Under Review). Wave, Tide and Topographical Controls on Headland Sand Bypassing. Submitted to: *Journal of Geophysical Research: Oceans*. Preprint available: https://doi.org/10.1002/essoar.10505252.1

Klopman, G. (1994). Vertical structure of the flow due to waves and currents. Progress report H840.30, Part II. Delft Hydraulics.

Lary, D. J., Alavi, A. H., Gandomi, A. H., & Walker, A. L. (2016). Machine learning in geosciences and remote sensing. *Geoscience Frontiers*, 7(1), 3–10.

Lee, T. R., Wood, W. T., & Phrampus, B. J. (2019). A machine learning (kNN) approach to predicting global seafloor total organic carbon. *Global Biogeochemical Cycles*, 33, 37–46. https://doi.org/10.1029/2018GB005992

Lee, T. R., Phrampus, B. J., Obelcz, J., Wood, W. T., & Skarke, A. (2020). Global marine isochore estimates using machine learning. *Geophysical Research Letters*, 47, e2020GL088726. https://doi.org/10.1029/2020GL088726

Leonardi, N., & Plater, A. J. (2017). Residual flow patterns and morphological changes along a macro- and meso-tidal coastline. *Advances in Water Resources*, 109, 290–301. https://doi.org/10.1016/j.advwatres.2017.09.013

Lesser, G. R., Roelvink, J. A., Van Kester, J. A. T. M. & Stelling, G. S. (2004). Development and validation of a three-dimensional morphological model. *Coastal Engineering*, 51(8), 883-915. https://doi.org/10.1016/j.coastaleng.2004.07.014

Levin, L. A. (1995). Influence of sediment transport on short-term recolonization by seamount infauna. *Marine Ecology Progress Series*, 123, 163-175. https://doi.org/10.3354/meps123163

Luijendijk, A. P., Ranasinghe, R., de Schipper, M. A., Huisman, B. A., Swinkels, C. M., Walstra, D. J. R., & Stive, M. J. F. (2017). The initial morphological response of the Sand Engine: A process-based modelling study. *Coastal Engineering*, 119, 1–14. https://doi.org/10.1016/j.coastaleng.2016.09.00

Martin, K. M., Wood, W. T., & Becker, J. J. (2015). A global prediction of seafloor sediment porosity using machine learning. *Geophysical Research Letters*, 42, 10,640–10,646. https://doi.org/10.1002/2015GL065279

MathWorks. (2020). *Statistics and Machine Learning Toolbox™ User's Guide*. September, 2020. Natick, MA: The MathWorks, Inc. Retrieved 29/10/2020: https://uk.mathworks.com/help/pdf_doc/stats/stats.pdf

McCarroll, R. J., Masselink, G., Valiente, N. G., Scott, T., King, E. V., & Conley, D. (2018). Wave and tidal controls on embayment circulation and headland bypassing for an exposed, macrotidal site. *Journal of Marine Science and Engineering*, 6(3), 94. https://doi.org/10.3390/jmse6030094

McCarroll, R. J., Masselink, G., Valiente, N. G., King, E. V. Scott, T., Stokes, C. & Wiggins, M. (Under Review). A general expression for wave-induced sediment bypassing of an isolated headland. *Coastal Engineering*. Pre-print: https://osf.io/preprints/eartharxiv/67rhx/download

McCarron, C. J., Van Landeghem, K. J. J., Baas, J. H., Amoudry, L. O. & Malarkey, J. (2019). The hiding-exposure effect revisited: A method to calculate the mobility of bimodal sediment mixtures. *Marine Geology*, 410, 22-31. https://doi.org/10.1016/j.margeo.2018.12.001

Nielsen, P. (1992). *Coastal bottom boundary layers and sediment transport*. Singapore: World Scientific Publishing Co. Pte. Ltd. https://doi.org/10.1142/1269

Németh, A. A., Hulscher, S. J. M. H., & de Vriend, H. J. (2003). Offshore sand wave dynamics, engineering problems and future solutions. *Pipeline & Gas Journal*, 230(4), 67.

O'Dea, E. J., Arnold, A. K., Edwards, K. P., Furner, R., Hyder, P., Martin, M. J., Siddorn, J. R., Storkey, D., While, J., Holt, J. T. & Liu, H. (2012). An operational ocean forecast system incorporating NEMO and SST data assimilation for the tidally driven European North-West shelf. *Journal of Operational Oceanography*, 5(1), 3-17. https://doi.org/10.1080/1755876X.2012.11020128

Olabarrieta, M., Medina, R., & Castenedo, S. (2010). Effects of wave–current interaction on the current profile. *Coastal Engineering*, 57(7), 643–655. https://doi.org/10.1016/j.coastaleng.2010.02.00

Pattiaratchi, C., & Collins, M. C. (1988). Wave influence on coastal sand transport paths in a tidally dominated environment. *Ocean & Shore Management*, 11(6), 449–465. https://doi.org/10.1016/0951-8312(88)90025-2

Phrampus, B. J., Lee, T. R., & Wood, W. T. (2020). A global probabilistic prediction of cold seeps and associated SEAfloor FLuid Expulsion Anomalies (SEAFLEAs). *Geochemistry, Geophysics, Geosystems*, 21, e2019GC008747. https://doi.org/10.1029/2019GC008747

Pingree, R. D., & Griffiths, D. K. (1979). Sand transport paths around the British Isles resulting from M2 and M4 tidal interactions. *Journal of the Marine Biological Association of the United Kingdom*, 59(2), 497–513. https://doi.org/10.1017/S0025315400042806

Pingree, R. D., & Griffiths, D. K. (1980). Currents driven by a steady uniform wind stress on the shelf areas around the British Isles. *Oceanologica Acta*, 3, 227–236. http://archimer.ifremer.fr/doc/00121/23265/

Pingree, R. D., & Le Cann, B. (1989). Celtic and Amorican slope and shelf residual currents. *Progress in Oceanography*, 23(4), 303–338. https://doi.org/10.1016/0079-6611(89)90003-7

Porter-Smith, R., Harris, P. T., Andersen, O. B., Coleman, R., Greenslade, D. & Jenkins, C. J. (2004). Classification of the Australian continental shelf based on predicted sediment threshold exceedance from tidal currents and swell waves. *Marine Geology*, 211, 1-20. https://doi.org/10.1016/j.margeo.2004.05.031

Reiss, H., Degraer, S., Duineveld, G. C. A., Kröncke, I., Aldridge, J., Craeymeersch, J., Eggleton, J. D., Hillewaert, H., Lavaleye, M. S. S., Moll, A., Pohlmann, T., Rachor, E., Robertson, M., vanden Berghe, E., van Hoey, G., & Rees, H. L. (2010). Spatial patterns of infauna, epifauna, and demersal fish communities in the North Sea. *ICES Journal of Marine Science*, 67, 278–293. https://doi.org/10.1093/icesjms/fsp253

780 Restreppo, G. A., Wood, W. T. & Phrampus, B. J. (2020). Oceanic sediment accumulation rates
781 predicted via machine learning algorithm: towards sediment characterization on a global
782 scale. *Geo-Marine Letters*, 40, 755–763.
783 https://doi.org/10.1007/s00367-020-00669-1

784 Ridderinkhof, W., Swart, H. E., Vegt, M., & Hoekstra, P. (2016). Modeling the growth and migration
785 of sandy shoals on ebb-tidal deltas. *Journal of Geophysical Research: Earth Surface*, 121,
786 1351–1372. https://doi.org/10.1002/2016JF003823

787 Roetert, T., Raaijmakers, T., & Borsje, B. (2017). Cable route optimization for offshore wind farms in
788 Morphodynamic areas. Paper presented at the 27th International Ocean and Polar
789 Engineering Conference, San Francisco, California, USA.

790 Scott, T., Masselink, G., O'Hare, T., Saulter, A., Poate, T., Russell, P., Davidson, M. & Conley, D.
791 (2016). The extreme 2013/2014 winter storms: Beach recovery along the southwest coast of
792 England. *Marine Geology*, 382, 224-241.
793 https://doi.org/10.1016/j.margeo.2016.10.011

794 Stride, A. H. (1963). Current-swept sea floors near the southern half of Great Britain. Quarterly
795 *Journal of the Geological Society*, 119(1-4), 175–197.
796 https://doi.org/10.1144/gsjgs.119.1.0175

797 Tambroni, N., Blondeaux, P., & Giovanna, V. (2015). A simple model of wave-current interaction.
798 *Journal of Fluid Mechanics*, 775, 328–348.
799 https://doi.org/10.1017/jfm.2015.308

800 Thompson, C. E. L., Williams, M. E., Amoudry, L., Hull, T., Reynolds, S., Panton, A. & Fones, G. R.
801 (2019). Benthic controls of resuspension in UK shelf seas: Implications for resuspension
802 frequency. Continental Shelf Research, 185, 3-15.
803 https://doi.org/10.1016/j.csr.2017.12.005

804 Tonani, M., Sykes, P., King, R. R., McConnell, N., Péquignet A-C., O'Dea, E., Graham, J. A., Polton, J. &
805 Siddorn, J. (2019). The impact of a new high-resolution ocean model on the Met Office
806 North-West European Shelf forecasting system. *Ocean Science*, 15, 1133–1158.
807 https://doi.org/10.5194/os-15-1133-2019

808 Tonani M. & Saulter, A. (2020). For NWS Ocean Waves Reanalysis Product
809 NWSHELF_REANALYSIS_WAV_004_015. Product User Manual. Issue 1.0. Copernicus Marine
810 Environment Monitoring Service.

811 Umeyama, M. (2005). Reynolds stresses and velocity distributions in a wave–current coexisting
812 environment. *Journal of Waterway, Port, Coastal and Ocean Engineering*, 131(5), 203–212.
813 https://doi.org/10.1061/(ASCE)0733-950X(2005)131:5(203

814 Uncles, R. J. (2010). Physical properties and processes in the Bristol Channel and Severn Estuary.
815 *Marine Pollution Bulletin*, 61(1-3), 5–20.
816 https://doi.org/10.1016/j.marpolbul.2009.12.010

817 Uncles, R. J., Clark, J. R., Bedington, M. & Torres, R. (2020). Chapter 31 - On sediment dispersal in the
818 Whitsand Bay Marine Conservation Zone: Neighbour to a closed dredge-spoil disposal site.
819 In J. Humphreys, R. W. E. Clark (Eds.), *Marine Protected Areas* (pp. 599 – 629). Amsterdam,
820 Elsevier.
821 https://doi.org/10.1016/B978-0-08-102698-4.00031-9

van der Molen, J. (2002). The influence of tides, wind and waves on the net sand transport in the North Sea. *Continental Shelf Research*, 22(18-19), 2739–2762. https://doi.org/10.1016/S0278-4343(02)00124-3

van Dijk, T. A. G. P., & Kleinhans, M. G. (2005). Processes controlling the dynamics of compound sand waves in the North Sea, Netherlands, Journal of Geophysical Research: Earth Surface, 110, F04S10. https://doi.org/10.1029/2004JF000173

van Leeuwen, S., Tett, P., Mills, D., and van der Molen, J. (2015), Stratified and nonstratified areas in the North Sea: Long-term variability and biological and policy implications, *Journal of Geophysical Research: Oceans*, 120, 4670– 4686. https://doi.org/10.1002/2014JC010485

Van Oyen, T. & Blondeaux, P. (2009). Tidal sand wave formation: Influence of graded suspended sediment transport. *Journal of Geophysical Research: Oceans*, 114, C07004. https://doi.org/10.1029/2008JC005136

Van Oyen, T., de Swart, H. & Blondeaux, P. (2011). Formation of rhythmic sorted bed forms on the continental shelf: An idealised model. *Journal of Fluid Mechanics*, 684, 475-508. https://doi.org/10.1017/jfm.2011.312

van Rijn, L. C. (2007a). Unified view of sediment transport by currents and waves. I: Initiation of motion, bed roughness, and bed-load transport. *Journal of Hydraulic Engineering*. 133(6), 649–667. https://doi.org/10.1061/(ASCE)0733-9429(2007)133:6(649

van Rijn, L. C. (2007b). Unified view of sediment transport by currents and waves. II: Suspended transport. *Journal of Hydraulic Engineering*, 133(6), 668–689. https://doi.org/10.1061/(ASCE)0733-9429(2007)133:6(668

van Santen, R. B., de Swart, H. & Van Dijk, T. A. G. P. (2011). Sensitivity of tidal sand wave characteristics to environmental parameters: A combined data analysis and modelling approach. *Continental Shelf Research*, 31(9), 966-978. https://doi.org/10.1016/j.csr.2011.03.003

Wang Z., Liang, B., Wu, G. & Borsje, B. W. (2019). Modeling the formation and migration of sand waves: The role of tidal forcing, sediment size and bed slope effects. *Continetal Shelf Research*, 190, 103986. https://doi.org/10.1016/j.csr.2019.103986

Ward, S. L., Neill, S. P., Van Landeghem, K. J. J., & Scourse, J. D. (2015). Classifying seabed sediment type using simulated tidal-induced bed shear stress. *Marine Geology*, 367, 94–104. https://doi.org/10.1016/j.margeo.2015.05.010

Wilson, R. J., Spiers, D. C., Sabatino, A. & Heath, M. R. (2018). A synthetic map of the north-west European Shelf sedimentary environment for applications in marine science. Earth System Science Data, 10(1), 109-130. https://doi.org/10.5194/essd-10-109-2018

Xu, K., Mickey, R. C., Chen, Q., Harris, C. K., Hetland, R. D., Hu, K., & Wang, J. (2016). Shelf sediment transport during hurricanes Katrina and Rita. *Computers and Geosciences*, 90(B), 24–39. https://doi.org/10.1016/j.cageo.2015.10.009

Zhang, W., Cui, Y., Santos, A. I., & Hanebuth, T. J. J. (2016). Storm-driven bottom sediment transport on a high-energy narrow shelf (NW Iberia) and development of mud depocenters. *Journal of*

Geophysical Research: Oceans, 121, 5751–5772.
https://doi.org/10.1002/2015JC011526